Membrane-associated σ factors disrupt rRNA operon clustering in *E. coli*

Khang Ho* and Rasika M. Harshey*

Department of Molecular Biosciences and

LaMontagne Center for Infectious Diseases,

The University of Texas at Austin,

Austin, Texas, 78712, USA

* Correspondence to either author: khang.ho@utexas.edu,

rasika@austin.utexas.edu

Abstract

Chromosomal organization in *E. coli* as examined by Hi-C methodology indicates that long-range interactions are sparse. Yet, spatial co-localization or 'clustering' of 6/7 ribosomal RNA (*rrn*) operons distributed over half the 4.6 Mbp genome has been captured by two other methodologies - fluorescence microscopy and Mu transposition. Our current understanding of the mechanism of clustering is limited to mapping essential *cis* elements. To identify *trans* elements, we resorted to perturbing the system by chemical and physical means and observed that heat shock disrupts clustering. Levels of σ^H are known to rise as a cellular response to the shock. We show that elevated expression of σ^H alone is sufficient to disrupt clustering, independent of heat stress. The anti-clustering activity of σ^H does not depend on its transcriptional activity but requires core-RNAP interaction and DNA-binding activities. This activity of σ^H is suppressed by ectopic expression of σ^D suggesting a competition for core-RNAP. A query of the other five known σ factors of *E. coli* found that elevated expression of FecI, the ECF σ factor that controls iron citrate transport, also perturbs clustering and is also suppressed by σ^D. We discuss a possible scenario for how these membrane-associated σ factors participate in clustering of distant *rrn* loci.

Introduction

Bacteria inhabit every available niche on earth, where they are subject to a range of environmental conditions to which they must acclimatize [1]. When conditions are favorable, bacteria quickly synthesize proteins required for uptake and biosynthesis of cellular building blocks that enable virtually every aspect of cell growth [2]. The bulk of cellular transcription during this phase is dedicated to *rrn* operons that synthesize ribosomes. Not only are *rrn* operons highly transcribed, but most bacteria also possess multiple such operons. The multiplicity of *rrn* operons has been correlated with elevated growth rate, genome integrity and acquisition of more diverse biosynthetic pathways [3,4], suggesting that there is an evolutionary advantage to maintaining multiple copies of these operons.

There are seven *rrn* operons in *E. coli* (*rrnA-G*), distributed on both arms (replicores) of the bi-directionally replicating chromosome, and residing in the upper half of each replicore [5] (S1 Fig). FROS (Fluorescent Reporter Operator Sites) experiments using pairwise *parS*-ParB interactions showed that 6/7 *rrn* loci spatially co-localize or cluster, reminiscent of the eukaryotic nucleolus [6]. This cluster was not detected by the more widely used Hi-C methodology, which employs formaldehyde to crosslink chromosomal interactions bridged by proteins [7]. Failure to detect the *rrn* cluster by this method could be due to disruption of the cluster by formaldehyde, or to a distance unfavorable for crosslinking. An alternative crosslinking method that exploits the natural mechanism of phage Mu transposition to link distant DNA sites indeed detected the *rrn* cluster [8]. The Mu method is not widely used as yet, because of the limited host-range of Mu, but has been additionally validated by corroborating the existence of a distinct Ter region on the *E. coli* genome [9] as demonstrated using other techniques [7,10].

The FROS study delineated *cis*-acting elements required for *rrn* clustering by systematically deleting regulatory regions upstream of *rrnD* and monitoring its co-localization with

rrnG, both located on the same arm of the chromosome but separated by 700 Kbp (S1 Fig) [6]. The study found that clustering required P1, the stronger of the two promoters driving transcription of *rrnD*, as well as an upstream binding site for the NAP (Nucleoid Associated Protein) Fis, but that neither Fis nor other NAPs known to regulate *rrn* transcription were required, suggesting that transcription of the *rrn* locus was not responsible for clustering. Consistent with this notion, mutation of the conserved -10 region of P1 failed to disrupt clustering, indicating that the formation of an open complex was also dispensable. Taken together, these results indicated that multiple transcribing RNA polymerases expected at these highly transcribed loci are likely not the cause of clustering. The Mu method showed that the NAP HUα and the condensin MukBEF influenced cluster formation, likely by affecting chromosome compaction in general [8].

To gain more insight into the phenomenon of *rrn* clustering we attempted to perturb the system by subjecting cells to amino acid starvation, as well as to heat, cold and ethanol shock. Of these, heat shock completely disrupted clustering. The heat shock response, part of the more general unfolded protein response [11], is designed to maintain heat-denatured proteins in a properly folded state, a key player in this response being σ^H [12]. σ^H (RpoH) regulates a large number of genes, notably those encoding protein chaperones such as GroEL/GroES [13,14]. We show that it is the rise in σ^H levels and not heat stress *per se*, that disrupts clustering, and we corroborate this observation using the Mu method. The observed σ^H-promoted de-clustering could be counteracted by simultaneous expression of σ^D (or σ^{70}). A similar but weaker effect on de-clustering was exhibited by FecI, which was also rescued by σ^D. Both σ^H and FecI are associated with the inner membrane. Based on these findings, we propose a model for how clustering of *rrn* operons occurs at the membrane and might be driven by the ability of sigma factor(s) to assemble RNAP onto cognate promoters.

Results

Heat shock disrupts *rrnA-rrnD* clustering

Gaal et al. used FROS to examine pair-wise combinations of fifteen of the possible twenty-one pairs of *rrn* operons, using distinct *parS*-ParB partners derived from phage P1 and plasmid pMT1 of *Yersinia pestis* [6,15]. In this study, we employed the same approach to determine *trans*-acting factors involved in clustering (Fig 1A). For our analysis we chose *rrnA* and *rrnD*, located on two different replicores (see Figs S1 and S2 for their relative location and for loci images, respectively), directing ParB-GFP 361bp upstream of *rrnA* and ParB-CFP 282 bp upstream of *rrnD* by inserting their respective *parS* sites at these locations; the median *rrnA-D* distance was estimated to be 134 nm. These cells were then subjected to various well-studied chemical and physical stresses (Fig 1B). Serine hydroxamate (SHX) is a serine analog that inhibits $tRNA^{Ser}$ aminoacylation, mimicking amino acid starvation and inducing a stringent response with concomitant synthesis of (p)ppGpp [16,17]. Application of this stress failed to produce a notable change (>2-fold) in the median *rrnA-D* distance (214 nm, compared to a significance cutoff at 230 nm; see figure legend for assignment of significance). Cold shock, which elicits changes in membrane fluidity, protein and nucleic acid folding and ribosome assembly [18], also did not significantly perturb clustering (216 nm). We note that since the resolution of our methods does not enable us to meaningfully distinguish distances below approximately 250 nm, distances below the cutoff are considered the same. Ethanol damages cell wall and membrane integrity, inducing an unfolded protein response in addition [11,19]. This stress increased the *rrnA-rrnD* distance to 424 nm. The unfolded protein response can also be produced by heat stress, which produced the most pronounced shift of the median distance relative to control (734 nm) (Fig 1B). Representative images from these experiments are shown in Fig 1C-D. We note that heat stress appears to localize *rrnA*, but not *rrnD*, to the pole, while also reducing the number of *rrnA* loci to 1 (Fig 1D, green arrow). Since

ethanol also induces the unfolded protein response, we infer that it is the unfolded protein response that promotes de-clustering of *rrnA* and *rrnD*.

Fig 1. Distance between *rrnA* and *rrnD* operons under various stress conditions. (A) Scheme for *rrn* operon tagging. Two different *par* sites (*parS*T1 and *parS*P1) were placed upstream of *rrnA* and *rrnD*, respectively, in the parent strain MG1655. These sites were visualized by co-expression of their cognate fluorescent ParB proteins (pMT1 GFP-ParB and P1 CFP-ParB). (B) Violin plots of the distance between *rrnA*-*rrnD* under indicated stress conditions (see Methods for details and S1 Table for strains and plasmids). The median distance (nm) between labeled loci is given below each graph. Between 400-900 foci are shown for each sample. The solid line indicates the median distance, and the top and bottom dashed lines indicate the 3rd and 1st quartile, respectively. We note that due to the large number of foci observed, a small change in the median distance is considered statistically significant ($p<0.001$) under Mann-Whitney test. The data shown are for one of three biological replicates. We arbitrarily considered a 2.5-fold change of median distance to be significant. We also note that since we have values that are 0, the border tries to encompass these data points, giving a false impression of negative distances. Data used for plotting this, and all other graphs can be found in the Supplemental “Raw Data” file under appropriate figure headings. (C) A representative image of *rrnA*-*rrnD* foci without added stress; many such images were used to generate data in (B). GFP and CFP were false-colored and enhanced for better visualization. One cell is outlined, with an arrow pointing to a merged GFP/CFP focus. The foci are edited in post-processing as a perfect circle to provide better contrast and visualization. Most cells appear to contain 2 copies of the *rrn* operons, indicating that this region of the chromosome is replicated. (D) Representative image of *rrnA*-*rrnD* de-clustering with heat stress. Panel labels as in C. Colored arrows indicate focus from either GFP-field (green) or CFP (red). We note that the number of *rrnA*-GFP foci is reduced to 1 focus per cell. See Methods for the code used to analyze fluorescent foci in this, and all similar figures.

Since our laboratory has shown that long-range contacts occur less frequently in an *hupA* (HUα) mutant [8], we also examined a noncoding (nc) RNA known to interact with HU [20]. A single deletion of nc5 showed no difference in the median distance between *rrnA* and *rrnD* (S3 Fig). RpoZ (an RNAP subunit) and NusB (a component of the anti-termination complex that interacts with RNAP), reported to contribute to phase-separation of *E. coli* RNAP [21], were also examined. Deletion of either *rpoZ* or *nusB* elicited a small increase (i.e. above our 2-fold cutoff of 230 nm) in the *rrnA-D* distance (254 nm and 304 nm, respectively) (S3 Fig), but not as drastic as that of heat stress.

In summary, of all the variables tested, heat stress caused the most significant de-clustering of the *rrnA-D* pair, followed by ethanol stress. These two stresses share the common outcome of producing an unfolded protein response.

Deregulation of GroEL/S disrupts *rrnA-rrnD* clustering

Since heat shock disrupted the *rrnA-D* pair, we hypothesized that some protein factor(s) bridging the two loci was displaced as a result. To identify bound proteins, we directed dCas9 (a variant of Cas9 capable of binding but not cleavage [22]), to upstream regions of all seven *rrn* loci, similar to the location of *parS* sites (see S2 Table), using the appropriate gRNAs. dCas9 was fused to 3X-FLAG, so anti-FLAG antibodies were used in pulldown experiments (S4A Fig). The efficiency of sgRNA targeting was determined by assessing lethality when Cas9 was provided instead of dCas9 (S5 Fig). Overall, in a host expressing Cas9, sgRNAs directed to all *rrn* operons caused a reduction in viability relative to a no-PAM control (S5 Fig). The differences in gRNA efficiency may influence the efficiency of dCas9 pulldowns, but since Cas9 targeting was productive, we concluded that the pulldowns would reflect at least the binding of dCas9 to the rDNA.

Mass spectrometry of the proteins identified in pull-downs with the seven *rrn* samples showed a range of significantly enriched proteins across different sgRNAs (z-score> 2.5, computed from three biological replicates for each sgRNA) using the methods described in [23]. For sgRNA targeting *rrnA, rrnB, rrnC, rrnD, rrnE, rrnG,* and *rrnH*, we found 54, 132, 135, 105, 66, 33 and 107 significantly enriched proteins, respectively (Figs S4B and S6). Common proteins identified across multiple samples are summarized in S7 Fig. The detailed spectral counts of identified proteins for each sgRNA can be found in S3-S9 Tables. No common protein was significantly enriched across all samples, but GroEL was enriched in 4/7 sgRNAs (*rrnC, rrnA, rrnB,* and *rrnD*), suggesting that GroEL could be a possible *trans*-acting factor in clustering. To control background protein abundance, we normalized *rrn* targeting samples to a gRNA targeting the non-*rrn* gene *lacZ* (with PAM) (see Methods). A potential pitfall of this approach is that we could not verify that clustering was preserved after formaldehyde crosslinking, due to loss of resolution of ParB foci after fixation, so it is possible that our data may not have sufficiently captured all the major players in clustering.

GroEL, in complex with GroES, acts as a chaperone for protein folding [24]. To investigate whether GroEL mediated the *rrn* clustering, we generated a chromosomal *groEL* deletion in the *parS*-tagged *rrnA-D* strain (S4C Fig). Since *groEL* is essential [25], we provided it in *trans* from a plasmid under control of pAraBAD and verified induction (with arabinose) and repression (with glucose) by observing corresponding increases and decreases in colony sizes, respectively (S8 Fig). Examination of the degree of *rrnA-rrnD* clustering under these two conditions showed that clustering was disrupted with arabinose addition (S4 Fig, third plot, red, from the left), even though GroEL levels were sufficient for growth as judged by colony size (S8 Fig); the median distance between *rrnA-D* increased to 494 nm. A WT 'control' carrying both *groEL*/*groES* under pAraBAD control increased *rrnA-D* distance to 216 nm (S4C Fig, second plot, yellow, from left); this slight increase is not significant based on our 2-fold cut-off, but the data nonetheless suggest that

ectopic expression *of groES/EL* affects clustering. Taken together, these results suggest that any perturbation of normal GroES/EL levels destabilizes clustering. Since these two genes are co-transcribed [26], we wondered if the imbalance in their relative levels was responsible for cluster disruption. We therefore placed the entire *groES/EL* operon on the plasmid vector in the Δ*groEL* strain, but that did not restore clustering either (S4C Fig, rightmost plot).

To test if expression of *groES/groEL* from their native σ^H-promoter (pGroE) would change the results, we compared *rrnA-D* distance when expression of this operon was controlled by pGroE vs pAra in both WT and Δ*groEL* strains (S4D Fig). In WT, pGroE had no discernable effect. In the Δ*groEL* strain, however, the *rrnA-D* distance shifted closer to normal with the pGroE plasmid as indicated by the 25% quartile of 242 nm for pGroE vs 356 nm for pAra (S4D Fig, compare rightmost two plots), suggesting that transcription from the native promoter was better at restoring clustering.

σ^H, also known as σ^{32} or RpoH, is the major heat shock sigma factor that transcribes the *groEL/S* operon exclusively [26]. Its levels are kept low through multiple mechanisms, including sequestration at the inner membrane, and direct interaction of GroEL/ES with σ^H [27,28]. Could our inability to restore *rrnA-rrnD* clustering in the Δ*groEL/ES* background be attributable to perturbation of σ^H levels? This was tested next.

σ^H disrupts *rrnA-rrnD* independent of its transcriptional activity

If perturbation of σ^H was the cause of *rrnA-D* de-clustering, we hypothesized that ectopic expression of σ^H alone should give similar results. We therefore placed *rpoH* under an inducible Tet promoter (pTc). Consistent with our expectations, *rpoH* induction increased the median distance between *rrnA-D* to 566 nm (Fig 2A, third plot from left). However, the same result was seen even in the absence of *rpoH* induction (Fig 2A, second plot from left). Unlike heat stress,

rpoH did not affect the number of *rrnA* foci (S9 Fig, compare to Fig 1D). To verify that *rpoH* was being expressed from the plasmid, we constructed a *lacZ* reporter driven from p*htpG*, a weak σ^H-responsive promoter [29], and assessed *lacZ* expression upon induction of *rpoH* from pTc (Fig 2B). A small but significant increase in β-galactosidase activity was observed after an hour of induction, the same time frame employed for microscopy (Fig 2A), indicating that *rpoH* was expressed from the Tet promoter. We conclude that even a small increase in σ^H levels promotes de-clustering of *rrnA*-*rrnD*.

Fig 2. **σ^H promotes de-clustering of *rrnA*-*rrnD* independent of its transcriptional activity** (A) Distance between *rrnA*-*D* with ectopic expression of *rpoH* from pTc (+). Induction was carried out for one hour prior to microscopy. In the 4th plot from left, *rpoD* is cloned downstream of TetR, from a constitutively expressed promoter, divergent from pTc. All other descriptions as in Fig 1. (B) Transcriptional activity of ectopically expressed *rpoH*. Miller assay was carried out as described in Methods. Student t's test was performed pairwise to determine statistical significance (two tailed, ns: not statistically significant, *: $p<0.05$, **: $p< 0.01$, ****: $p< 0.0001$). (C) Distance between *rrnA*-*D* with ectopic expression of indicated *rpoH* mutants, compared to empty vector control. (D) Transcriptional activity of ectopically expressed *rpoH* mutants, as described in B.

To ascertain that the data in Fig 2A are not merely due to perturbation of cellular morphology and nucleoid structure, we measured both, under both heat stress and *rpoH* induction. Under the heat stress, cell lengths showed a small but statistically significant increase: 2.9µm on average compared to 2.8µm for the control (S10A Fig). Under *rpoH* overexpression, cell lengths decreased on average to 2.5µm compared to 2.8µm for the control. To determine the effect of these perturbations on the nucleoid, we performed DAPI staining under these conditions. Curiously, we found that the nucleoid is more condensed, not decondensed, under both conditions (S10B Fig). These results indicate that the de-clustering effect of heat stress or *rpoH* expression is not a consequence of changes in nucleoid compaction or cellular morphology. As

another control to ascertain that the change in *rrnA-D* distance was specific to these loci and not due to a general increase in distance between any two loci, we tagged *lacZ*-pMT*parS* and *leuC*-P1*parS* (200 Kbp apart; S10C Fig, left) and measured their distance -/+ *rpoH* expression (S10C Fig, right). We observed no change in their distance between the two conditions.

E. coli possesses seven experimentally confirmed sigma factors, of which the vegetative σ^D (RpoD or σ^{70}) is the most abundant [30]. Since the amount of RNAP is thought to be relatively constant across most growth conditions, competition among the sigma factors for this core RNAP has been proposed to be the mechanism for gene regulation [30,31]. To test if competition between σ^H and σ^D for binding RNAP could be responsible for destabilizing clustering, we inserted *rpoD* downstream of TetR on the same plasmid, which is driven by the constitutive promoter divergent from pTc (pTetR). Expression of *rpoD* decreased the median distance between *rrnA-D* to 213 nm compared to 566 nm with the *rpoH* vector alone (Fig 2A, compare fourth plot to second plot from the left), supporting the notion that competition between σ^D and σ^H for core RNAP likely suppressed the de-clustering activity of σ^H.

To test this notion further, we examined the following previously characterized mutants of *rpoH,* reported to have decreased or increased transcription activities: L245P is defective for interaction with RNAP [32], E265A is defective for promoter binding at the -35 region [32], and I54N has increased stability [28,29]. Our expectation was that the L245P and E265A would lose their de-clustering activity, while I54N mutant would not. This expectation was borne out for the L245P and E265A variants (303 nm and 216 nm, respectively), but not for I54N (284 nm) i.e. all three variants were defective in destabilizing the *rrn* cluster, compared to WT RpoH (566 nm) (Fig 2C). We note that in contrast to cells expressing the first two variants, those expressing I54N are elongated (S11 Fig). I54N has been shown to exhibit elevated transcriptional activity due to its inability to localize to the membrane like WT σ^H [27,29], which likely perturbs normal cell physiology. The expected transcriptional activity of all the σ^H mutants was confirmed using the

lacZ reporter as before (Fig 2D). We conclude that σ^H -mediated de-clustering is independent of its transcriptional activity.

σ^H does not disrupt all *rrn* pairs

Our experiments thus far queried the co-localization of the *rrnA-D* pair as representative of all the *rrn* loci found in the cluster [6]. To test if heat shock and σ^H were equivalent in their disruptive ability, we decided to query other pairs, including every co-localizing *rrn* operon at least once, with *rrnC* as the non-clustering control. Heat shock disrupted clustering of all non-C *rrn* operons tested, the median distance increasing 1.5 - 2.5 fold (from 80-120 nm to 450-700 nm) (Fig 3A; summary of the results is diagrammed in Fig 3B). *rrnC* is reported to not be part of the cluster [6,8], yet its distance from *rrnG* remained curiously unperturbed by heat, staying at ~400nm median, suggesting perhaps a specificity to clustering that is immune to the global effect of heat stress.

Fig 3. Disruption of *rrn* clustering by heat stress and by FecI. (A) Effect of heat stress on clustering of indicated *rrn* pairs. Other descriptions as in Fig 1. (B) Schematic summary of data in A. Each of the 7 *rrn* operons was visited at least once. (C) Response to *rpoH* induction of tested *rrn* pairs. +/- symbols are self-explanatory. (D) Effect of induced ectopic expression of five σ factors on *rrnA-D* distance, all placed under control of pTc with the same RBS.

The effect of RpoH on the *rrn* pairs tested was non-uniform (Fig 3C). Specifically, we observed that two pairs that shared *rrnH* appeared to be resistant to disruption by σ^H (Fig 3C). Thus, contacts between all the *rrn* loci in the cluster are not uniform, suggesting that there is likely a sub-organization within this structure.

To determine if σ^H played a unique role in affecting cluster stability, we ectopically expressed the other five sigma factors: RpoE (σ^{24}), RpoF (σ^{28}), RpoN (σ^{54}), RpoS (σ^{38}) and FecI (σ^{19}), under the same promoter as the *rpoH*-expressing vector, maintaining the same RBS

(ribosome binding site). Of these, FecI produced a smaller (compared to RpoH) destabilizing effect (134 nm vs 234 nm; Fig 3D). To test if σ^D would restore clustering to the FecI-expressing strain like it did when co-expressed with σ^H (Fig. 2A), we co-expressed *rpoD* with *fecI*; clustering was completely restored to WT levels (Fig 3D, compare last two plots). We note that the shared properties of RpoH and FecI are that they are both normally sequestered at the inner membrane, suggesting perhaps that *rrn* clustering may have a membrane component.

σ^H disrupts the *rrn* cluster as tracked by the Mu method

Phage Mu transposition requires direct contact between Mu and its transposition target and displays virtually no sequence specificity in its target choice [33]. Higher or lower frequencies of transposition are therefore interpreted to reflect higher or lower rates of physical contact between the interacting chromosomal regions, analogous to the contact frequencies inferred from normalized Hi-C data [34]. Contacts made by Mu when located next to *rrnD* showed significantly positive interaction between *rrnD* and chromosomal regions containing *rrnA, B, E, G, and H* (but not *rrnC*), suggesting physical proximity of these regions, as also seen by FROS [6].

Since we did not examine the effect of σ^H on all possible combinations of *rrn* loci with FROS (Fig 3C), we used the Mu method to examine transposition patterns of Mu located near *rrnD* in the presence of ectopically expressed RpoH. The pattern of Mu transposition from the *rrnD*-proximal locus in WT cells was consistent with the earlier report, where Mu could access every region of the chromosome irrespective of its starting location (Fig 4A). In the presence of the vector encoding RpoH, even without induction of RpoH expression, the transposition landscape was altered, with more Mu insertions now occurring proximal to the starting Mu in Bin 72 (Fig 4B). This increase in local versus distal contacts is exacerbated with *rpoH* induction (Fig 4C). Transposition frequencies across different conditions are summarized in Fig 4D. We

observed that with expression of *rpoH,* Mu predominantly inserts in its starting bin (yellow bar, indicating highest transposition frequency, seen only in the RpoH and +RpoH data), with insertions to distant bins decreased (darker blues in +RpoH and RpoH columns compared to No Vector) (Fig 4D). We conclude that *rpoH* overexpression disrupts long range contacts.

Fig 4. Expression of *rpoH* disrupts *rrn* clustering as tracked by Mu transposition. (A) Frequency of transposition of Mu located in the vicinity of *rrnD* (Bin 73) after one round of transposition. The number of insertions has been normalized to the read depth of each bin but not normalized to copy number. In the asynchronous population, many cells have partially replicated chromosomes [8]. The initial Mu position is indicated by a red triangle. The *E. coli* genome was partitioned into 100 equally sized bins, so each bin is ~46 kb. Starting Bin number and chromosomal regions are indicated on top. Each vertical bar represents the average normalized transposition frequency of 3 biological replicates at the indicated bin, expressed as a percentage (with the highest transposition frequency being set to 100%). Grey error bars are the standard deviation. Color of bars correspond to regions of the *E. coli* chromosome annotated up top [8]. (B) Same as (A) but with the *rpoH* vector. (C) Same as (B) but with induction of *rpoH*. (D) Heat map of the data from A through C. In the no-vector control, the highest insertion frequency (yellow bar) occurs in Bin 94 (close to *oriC* which resides in Bin 90). (E-J) Transposition frequency from *mlaF* (*rrnD*) into the indicated *rrn* operon-containing bin under conditions described in A through C. The individual data points and associated standard deviations are shown. Statistical significance was determined with Student t's test (two-tailed), *: $p<0.05$. ns: not statistically significant. (K) Model for σ^D-mediated *rrn* clustering**.** σ^D-bound RNAP (dark green) is responsible for clustering *rrn*s (blue circles) at the membrane either directly or through other unknown factor(s) (grey hexagon). GroEL/ES (red oval) represses the activity of σ^H (orange) preventing it from competing with σ^D for core RNAP. σ^H is typically localized to the inner membrane and degraded. Upon heat stress, σ^H levels rise, and GroEL/ES, being diverted to un-folded substrates (pink oval),

is unable to repress σ^H activity. Elevated σ^H levels from a plasmid, phenocopy the heat response. σ^D-bound RNAP complexes are displaced through competition with increased σ^H, and σ^H-bound RNAP now transcribes genes in σ^H regulon (green circles), lowering the total amount of RNAP transcribing *rrn* operons at the membrane, destabilizing clustering.

We next specifically examined the bins containing *rrn* operons to assess the effect of RpoH on Mu transposition. We observed that contact between *rrnD* and a majority of the *rrn* loci decreased (Fig 4 E,F,H,J), with the notable exception of those with *rrnC* and *rrnH*, which remained unchanged (Fig 4G and I). The *rrnC* result is consistent with earlier reports [6,8], and the *rrnH* result is consistent with data in Fig 3C, where RpoH promoted de-clustering of all *rrn* examined, with the exception of *rrnH*. Overall, the Mu transposition data support the hypothesis that σ^H promotes de-clustering of *rrn* operons.

Discussion

This study demonstrates that the *E. coli* 'nucleolus' where 6/7 *rrn* operons are reported to co-localize, can be perturbed by the cellular heat shock response as demonstrated by both FROS and Mu transposition. This perturbation is not due to heat stress per se, but rather due to elevation of RpoH or σ^H levels known to occur during the response. We discuss below what this and other data may suggest about the mechanism of co-localization of the *rrn* operons.

Ability to disrupt its organization validates the existence of the *E. coli* 'nucleolus'

In eukaryotic cells, the nucleolus is the primary site of ribosome biogenesis [35]. It is a large structure, where hundreds to thousands (depending on the organism) [36] of rRNA operons localize, a device thought to have evolved to maximize translation efficiency [35]. By contrast, *E.*

coli has only seven operons encoding ribosomal DNA (*rrn* operons) [37] (S1 Fig), 6/7 of which were observed to come together in some unknown fashion as reported by two completely different methodologies – FROS and Mu transposition [6,8]. Gaal et al. (FROS methodology) called this organization a 'bacterial nucleolus' and showed that its presence was independent of growth media and of cell doubling times [6]. Although the stronger of the two promoters, P1, and it UP element in *rrnD*, were required, active *rrn* transcription was ruled out because co-localization of the loci queried was resistant to disruption by rifampicin, which stops RNA chain elongation [38], as well to mutation of a -10 region of the P1 promoter required for initiation of transcription. These properties of the *E. coli* nucleolus are in contrast to the requirement for Pol I function and rRNA transcription to maintain nucleolar structure and integrity in eukaryotic cells [39]. We will therefore simply call this co-localization a *rrn* cluster.

To learn more about the nature of the *rrn* cluster, we attempted to perturb it by exposing cells to several environmental stressors (Fig 1B). Of these, heat and ethanol shock had the largest effect. These two stressors share a common 'unfolded protein' response [11]. The important take-away from this experiment is that by perturbing the cluster, we had not only validated its existence but found a handle to probe its nature.

The heat shock response, GroEL/GroES and σ^H all destabilize the *rrn* cluster: σ^D counteracts the action of σ^H

Adaptation to heat shock is a universal biological phenomenon [11]. Heat denatures proteins, so organisms adapt by synthesizing protein-folding chaperones. *E. coli* encodes several chaperones including GroEL/GroES and employs σ^H to transcribe hundreds of genes that enable bacterial survival [13,14]. The ability of heat shock to disrupt the *rrn* cluster (Fig 1B-D) suggested to us that proteins must participate in holding the structure together at some level. We therefore directed

FLAG-tagged dCas9 immediately upstream of each of the 7 *rrn* loci, followed by pull-down with FLAG antibodies and mass spectroscopy. No common protein was significantly enriched across all samples, but GroEL was enriched in 4/7 sgRNAs (*rrnC, rrnA, rrnB,* and *rrnD*), suggesting that GroEL could be a possible *trans*-acting factor in clustering (Figs S4B and S6-7). (Although *rrnC* is not part of the cluster, it is close to the origin of replication *ori*, and it is conceivable that unrelated events at *ori* block its incorporation into the cluster).

The *groEL/S* operon is transcribed exclusively by σ^H, whose levels are kept low through multiple mechanisms, including sequestration at the inner membrane where it is degraded by protease FtsH, as well as direct interaction with GroEL/ES [27,28]. Attempts to query the participation of GroEL by providing it either from regulated promoter or its native promoter resulted in disruption of the *rrn* cluster (S4C-D Fig). To test if our manipulations of GroEL were perturbing σ^H levels, we provided RpoH ectopically from a regulatable promoter. Even in the absence of induction, leaky expression of RpoH was sufficient to disrupt the *rrn* cluster (Fig 2A).

Why should an apparently slight rise in σ^H levels have such a profound effect on stability of the cluster? Given that the P1 promoter and its UP elements somehow participate in maintaining the cluster, we imagined a scenario where RNAP bound to the housekeeping σ^D, known to transcribe the *rrn* operons [5], was stationed there, and that σ^H might be competing with it for binding RNAP, displacing it and disrupting the structure. Testing this conjecture by inserting *rpoD* along with *rpoH* on the ectopic vector resulted in significant cluster rescue (Fig 2A), supporting our conjecture.

Sigma factors that disrupt the *rrn* cluster associate with the membrane, suggesting a model for *rrn* clustering

Competition among sigma factors for the core RNAP has been proposed to be the mechanism for gene regulation [31]. If such a competition model applies to why rise in σ^H disrupts the cluster, then mutants of σ^H that are defective for either RNAP-core or DNA-binding should not disrupt the cluster. RpoH mutants defective for interaction with RNAP (L245P) and for promoter binding at the -35 region (E265A), were both significantly deficient in the de-clustering activity of WT RpoH (Fig 2C), in keeping with the competition model.

σ^H levels are regulated by at least three mechanisms: control through GroEL/GroES, DnaJ/K/GrpE, control of translation efficiency at the mRNA level, and the degradation of σ^H by FtsH, an integral-membrane protease. A third RpoH mutant we tested for its de-clustering activity was I54N, shown to escape FtsH-mediated proteolysis. Our expectation was that this mutant would behave like WT RpoH. Despite its high transcription activity (Fig 2D), however, the effect of the I54N mutant did not align with our expectations (Fig 2C), showing at the very least that high levels of transcription directed by σ^H are not the cause of de-clustering, and that none of the members of the σ^H regulon are involved in de-clustering. So why did the I54N mutant not behave like WT RpoH? Unlike the WT protein, I54N mutant is unable to localize to the membrane, suggesting that access to the membrane is important for the de-clustering effect of RpoH, ergo, the *rrn* cluster might be anchored in the membrane.

Of the five other sigma factors tested for cluster-disrupting ability, only FecI, an extracytoplasmic- function (ECF) σ factor, also disrupted clustering, although not as severely as σ^H (Fig 3D). FecI, along with FecA and FecR, is responsible for the transcription of the ferric citrate transport system, consisting of *fecABCDE* transport genes [40]. FecA is an outer membrane protein that transports $(Fe^{3+}\text{-citrate})_2$ across the outer membrane. Upon binding of $(Fe^{3+}\text{-citrate})_2$ to FecA, the signal is then transduced through the periplasmic face of FecR, an inner membrane protein, to its cytoplasmic face [41,42]. This conformational change of FecR activates the transcriptional activity of FecI in the cytoplasm and promotes transcription of *fecABCDE* [43]. The

dependence of FecI on FecR, which is localized to the inner-membrane, for efficient transcription by RNAP-FecI of the *fec* operons, also lends support to a model where the site of *rrn* clustering is the inner membrane. Why then did overexpression of σ^E, which is also an ECF, fail to disrupt clustering [44,45]? The mode of regulation of σ^E is based on the repression of σ^E by the inner membrane anti-sigma factor RseA, inhibiting the interaction of RNAP core and σ^E [46,47]. Upon membrane stress, such as ethanol or heat, DegS is activated by the presence of unfolded outer-membrane proteins, and, in concert with RseP, degrades RseA, releasing σ^E to promote transcription of downstream genes [48,49]. The negative regulation by RseA may explain why overexpression of σ^E alone is unable to disrupt clustering. In other words, for efficient disruption of the *rrn* cluster, σ^D-independent transcription needs to occur <u>at</u> the inner membrane.

Taken together, we propose that clustering of *rrn* is mediated by σ^D at the membrane either through σ^D directly or through other unknown factor(s) (Fig 4K). σ^D has indeed been observed at the membrane [28]. Given that high levels of transcription are not required, but the *cis*-acting elements responsible for high transcriptional activity of *rrn* are, and that some σ factors can disrupt clustering implicating σ^D as the clustering factor, we propose that the assembly of RNAP holoenzyme and UP element features of P1 drives *rrn* clustering. Upon heat stress or elevated σ^H levels, RNAP complexes bound to σ^D are displaced through competition with σ^H, and to a lesser extent FecI, for RNAP core, resulting in de-clustering of *rrn* operons. The order of RNAP assembly has been shown to be $\alpha_2 \rightarrow \alpha_2\beta \rightarrow \alpha_2\beta\beta'\omega \rightarrow \alpha_2\beta\beta'\omega\sigma$ [50]. The requirement for the P1 promoter may reflect the high affinity of α for the UP element present upstream of the -35 element [51]. The dimerization of the α subunit could drive the bridging interaction between the disparate *rrn* operons. However, this interaction by itself is unable to explain *rrn* clustering as demonstrated by de-clustering effect of σ^H and FecI, since σ factor binding and unwinding of the DNA duplex is the last step of RNAP assembly. Therefore, we propose that two elements are responsible for *rrn* clustering: (1) the high affinity of α for the UP element, and (2) DNA binding driven by σ^D. The

affinity of α for the *rrn* UP element would explain why *rrn* clustering does not extend to other non-*rrn* loci. The specificity of σ^D for the *rrn* promoter would explain the de-clustering activity of σ^H and FecI. We note that σ^H did not affect the position of two pairs that shared *rrnH* (Fig 3C), suggesting a likely sub-organization within this structure. Finally, why did we recover GroEL at 4/7 rDNA loci (Figs S4A-C and S6-7)? One possibility is that GroEL is meant to clear σ^H from the cluster [27]. Alternatively, since GroEL has been shown to restore transcription of heat-treated RNAP *in vitro* [52], it could either be interacting non-specifically with some component of RNAP or ensuring that the proteins at the cluster do not aggregate.

Relationship of the *rrn* cluster to RNAP condensates

RNAP has been reported to form distinct clusters on the *E. coli* nucleoid [53,54]. Since the bulk of cellular transcription is dedicated to rRNA transcription and since RNAP clusters form in fast-growth conditions, it was proposed that these clusters represent high concentrations of RNAP on *rrn* operons [55]. Subsequent work showed that RNAP clusters colocalize with nascent rRNA, but that their spatial arrangement was not dependent on rRNA synthesis activity and was likely organized by the underlying nucleoid [56]. RNAP clusters have been shown to be biomolecular condensates capable of phase separation, involving known factors associated with RNAP (i.e. ω subunit of RNAP and NusB) [21].

The properties of the *rrn* cluster are on the one hand reminiscent of RNAP condensates in that high level of transcription of rRNA is not required for their organization, but, on the other hand, are different in that the cluster is immune to transcription inhibitors while the condensates are not [56]. The cluster is unlikely to serve as a precursor for formation of RNAP condensates since these form in a strain where only one *rrn* operon is present [48]. Antitermination factors such as NusB and ω subunit of RNAP have been shown to contribute to formation of RNAP

condensates [23]. However, we showed in this study that neither Δ*nusB* nor Δ*rpoZ* strains significantly impact the cluster (S3 Fig). We interpret these results to mean that RNAP condensates represent a feature of highly active transcription that the *rrn* cluster contributes to by making rDNA readily available through spatial localization.

Acknowledgments

We thank Rick Gourse for providing pFHC2973 and *parS*-labelled *rrn* strains, Ian Molineux for BW25141 for propagation of R6K origin plasmids, Kamyab Javanmardi for providing Golden Gate vector for gRNA insertion, Rachael Cox and Edward Marcotte for script and computing power used in mass spectrometry analysis, Brady Wilkins for assistance with Southern Blot, and Lydia Freddolino for comments on the manuscript. Figures were created with Biorender. This work was supported by NIH grant GM118085. Partial support was provided by Robert Welch Foundation (F-2190).

Materials and Methods

Media, Strains, Phages and Plasmids. Unless conditions are specified, all strains are grown in LB at 30°C with shaking. When appropriate, antibiotics were at the following concentrations: Ampicillin (Amp) at 100µg/mL, Kanamycin (Kan) at 25µg/mL, Chloramphenicol (Cam) at 20µg/mL. Anhydrotetracycline (aTc) was used for induction of Tet promoter at 50ng/mL. Isopropyl-β-D-Galactoside (IPTG) was used to induce the *lac* promoter at 1mM. O-nitrophenyl-β-D-Galactoside (ONPG) was purchased from Sigma. Competent cells for transformation were prepared by washing a growing culture of O.D. 0.4-0.5 in cold 10% glycerol 3 times. The pellet was resuspended in 1:100 of the original volume in 10% glycerol. Electroporation was performed in *E.*

coli Pulser (Biorad) with 1mm Electroporation cuvette Plus (Fisher) at 1.8V. Cells were recovered in SOC (LB supplemented with 10mM $MgCl_2$, 10mM $MgSO_4$, and 0.2% Glucose) for 1.5 hours at 30°C with shaking prior to plating on the appropriate selection. Mu phage was stored in Mu Buffer (50mM Tris-HCl pH 8.0, 100mM NaCl, 5mM $CaCl_2$, 5mM $MgCl_2$, and 0.1% gelatin). Strains and Phages employed in this study are listed in S1 Table. Primers, purchased from Integrated DNA Technology (IDT), used in this study are listed in S2 Table.

General Molecular Techniques. Routine PCR was performed with Taq DNA Polymerase (NEB), according to manufacturer's instructions. PCR fragments for cloning were generated with Phusion DNA Polymerase (NEB) according to manufacturer's instructions. Gibson Master Mix was made according to Gibson *et al* [57]. Gibson assembly was performed at 50°C for at least 2 hours. Golden Gate Assembly was performed with Esp3I (NEB), T7 DNA Ligase (NEB), T4 DNA Ligase Buffer (NEB). Primers used to generate gRNAs were used at 10nM each. 100ng of the destination vector (pMAZ-SK sfgfp) was used. The program for Golden Gate Assembly was 3 minutes at 37°C, 2 minutes at 16°C for 35 cycles, followed by 1 cycle of 10 minutes incubation at 37°C. T4 DNA Ligase, T4 Polynucleotide kinase (PNK), and T4 DNA Ligase Buffer were purchased from NEB.

Plasmid Construction. Plasmids were constructed using Gibson assembly. Typically, 250µL of the backbone was assembled with a molar equivalent of insert in a 20µL reaction. The resulting product was purified with PCR clean-up kit (Qiagen) according to the manufacturer's instructions. 2µL of the 20µL eluted product was used for transformation. Colonies were screened by PCR with primers spanning the junction between the backbone and the insert. Positive clones were restruck and checked once more using the same primer pairs. The PCR product was sequenced to confirm the identity of the sequence at either the UT Core Sequencing Facilities or Eton Biosciences. For generating single point mutants, primers carrying the desired mutation were used to amplify the plasmid of interest. The resulting PCR product was gel-extracted with Qiagen

Gel Extraction Kit. The product was then self-ligated overnight with T4 DNA Ligase and T4 DNA PNK in T4 Ligase Buffer. The ligated product was then purified and 2µL of the 20µL eluted product was used for transformation. Positive clones carrying the desired mutation were identified by PCR of the target sequence followed by sequencing. The positive clones were then restruck once again and verified with PCR and sequencing.

Strain Construction. For insertion of *parS* sequences, the procedure was essentially as described in [58] with the exception being the template plasmid (pKH3 or pKH4) carrying the appropriate *parS* linked to antibiotic resistance cassette. Briefly, 0.5mL of an overnight culture of MG1655 carrying pKD46 was pelleted, washed twice in 1mL of PBS, and diluted 1:100 in fresh LB supplemented with 0.2% arabinose. The culture was grown to an O.D. of approximately 0.4. The cells were made electrocompetent. Cells were then transformed with the appropriate PCR product and let recover in SOC for 3 hours at 30°C. The outgrowth was then plated on the appropriate selection and incubated at 37°C overnight. Positive clones were identified by PCR with primers amplifying the junction of the expected insertion. Positive clones were struck out on the appropriate selection plate at 37°C and reconfirmed with PCR followed by sequencing. To remove the antibiotic-encoding cassette for subsequent insertion of additional *parS*, pCP20 was transformed into the desired host strain. Clones carrying pCP20 were then struck out on LB plate without selection and incubated at 42°C overnight. Colonies were then checked for the loss of both pCP20 and the antibiotics cassette by streaking on the appropriate selection.

Fluorescent Microscopy and Post-Processing. Overnight cultures used for fluorescent microscopy were grown overnight in EZ-Rich media (Teknova) from a single colony and diluted 1:100 in fresh EZ-Rich media supplemented with IPTG for induction of ParB-fluorescent fusions from pFHC2973. The subculture grew until an O.D. of 0.4. 1mL of the culture was then pelleted by centrifugation and resuspended in 100µL of PBS. 6uL of the suspension was then spotted onto agarose pad (1%) and let dry. The sample was then observed under Olympus-BX 53 microscope,

XM10 monochrome camera on the 100x objective with oil immersion. Most images were taken at an exposure of ~100ms for GFP filter, and ~400ms for CFP filter, however, some samples required a longer exposure time to obtain acceptable signal for downstream processing; the upper limit of exposure was 3s. Cellular stressors were applied 20 minutes prior to imaging, after which they were prepared and imaged as described above. For heat stress, the cells were transferred to a 42°C water bath. SHX was added to a concentration of 50µM. Cold stress was induced by incubating the cells in a 4°C water bath. Ethanol stress was induced by adding ethanol to 0.5%. For image-processing, the background was subtracted from the image, and foci were detected with ImageJ using the detect maxima function. The coordinates of the foci were exported and the Cartesian distance between a GFP focus, and its closest CFP focus was determined with custom Python script. The distance was computed by scaling the distance in pixel to nm with 1 pixel = 62nm. Cell length was measured with ImageJ using the same scale as described above (1pixel = 62nm). For each experiment, three biological replicates were examined, and one representative is shown. Code used for analyzing the foci can be found at 10.5281/zenodo.14927315.

DAPI Staining and Nucleoid Measurements. Cells were grown and subjected to heat stress or *rpoH* expression in manner identical that used for microscopy. 1mL of cells were then washed twice in PBS and resuspended in 200µL of diH_2O. 37% Formaldehyde (Fisher) was added to a final concentration of 3.5% and incubated at 4°C for 30 minutes, after which time, the cells were washed 3 times in 1mL of PBS and resuspended in DAPI solution (500nM in diH_2O, 200µL) for 10 minutes. The cells were then washed once in 1mL of PBS, resuspended in 100 µL of PBS, mounted for microscopy and visualized with DAPI filter. The signal intensity for DAPI was measured by ImageJ.

Pulldown of dCas9 and Proteomics. Three independent overnight cultures of MG1655 carrying pKH5 and the corresponding gRNA were pelleted and washed as described above. The pellet was diluted 1:100 into 100mL fresh LB supplemented with selection and 0.2% arabinose and aTc.

The cultures were grown to an O.D. of 0.6 and pelleted and washed 3 times in 1mL of PBS. The subsequent pulldown procedure was carried out as described by FLAG Immunoprecipitation kit (Rockland). Every step of the pulldown was conducted at 4°C. Briefly, the pellet was resuspended in 5mL of lysis buffer and sonicated (Brason tip, 40% intensity) for 10 minutes (10s on, 10s off cycle). The lysate was clarified by centrifugation at 4°C. Agarose-αFLAG Ab was washed twice in PBS and once in elution buffer. The washed Agarose-αFLAG Ab was incubated with the lysate overnight. After incubation, the beads were collected and washed 3 times with PBS. The bound proteins were eluted with elution buffer. The proteins were quantified by Mass Spectrometry at the UT Proteomics core. Samples were digested with trypsin, desalted and run on Dionex LC (liquid chromatography) and Orbitrap Fusion 2 (mass spec machine) for 60 minutes. Raw data were analyzed with PD2.2 and Scaffold 5 software. Downstream analysis was performed as described in [23] with *lacZ* gRNA pulldown as the negative control. Significantly enriched hits were ranked based on a z-score cut-off of 2.5.

Miller Assay. 0.5mL of three overnight cultures of the desired strain carrying the appropriate plasmid was pelleted and washed in 1mL of PBS twice. The pellet was then resuspended in 0.5mL of PBS and diluted 1:100 in LB. The cultures were grown to an O.D. of 0.4 and aTc was added. At indicated time points, 20µL of the culture was withdrawn, its O.D. 600 recorded and added to 80µL of permeabilization buffer (100mM $NaHPO_4$, 20mM KCl, 2mM $MgSO_4$, 0.8mg/mL CTAB, 0.4mg/mL sodium deoxycholate, 5.4µL/mL β-mercaptoethanol). After the final time point, 600µL of substrate solution (60mM Na_2HPO_4, 40mM NaH_2PO_4, 1mg/mL ONPG, 2.7µL/mL β-mercaptoethanol) was added to each sample. The samples were incubated at 30°C for 60 minutes before 600µL of 1M Na_2CO_3 was added to stop the reaction. O.D. 420 was recorded. Miller units were calculated as follows:

$$Miller\ Units = 1000 \times \frac{Absorbance_{420nm}}{60 \times Absorbance_{600nm} \times 0.02}$$

Mu Phage Preparation. When required, a Mu prophage strain was grown overnight, diluted 1:100 in fresh LB and grown until an O.D. of 0.5. After which, the culture was shifted to a 42°C water bath and incubated until lysis is complete. The lysate was clarified by centrifugation at 6000g for 20 minutes. The supernatant was transferred to a clean flask and NaCl was added to a final concentration of 0.5M followed by the addition of Polyethylene Glycol 8000 to a final concentration of 10% w/v. The mixture was incubated overnight at 4°C. The pellet was then collected by centrifugation at 8000g for 20 minutes. The pellet was then resuspended in 1:100 of the original volume in Mu Buffer. Chloroform was added to the mixture and shaken. The phases were separated by centrifugation at 4000g for 10 mins at 4°C. The aqueous phase was collected (top layer) and phage titer determined prior to use.

Generation of mlaF::Mu and single-transposition experiments. Selection for Mu insertion at *mlaF* (bin72 as described in [8]) was performed by first introducing *sacB* at *mlaF* followed by infection Mu carrying a Cam marker. Briefly, *attP* was introduced into *mlaF* by λred recombination, and the Kan marker was removed. KH2 was then introduced into this strain, induced for expression of λ Int with arabinose followed by transformation of KH22. Clones positive for integration of the *sacB-kanR* cassette was verified by PCR spanning the expected junction between the cassette and *mlaF*. This strain was then infected with Mu::Cam at an MOI (multiplicity of infection) of 5, and survivors that were resistant to sucrose and Cam were selected for. Three colonies were picked and insertion locations for each were confirmed with PCR. Southern Blot was performed to confirm that only one Mu inserted at the desired location. Of 3 clones picked, one was confirmed to be a mono-lysogen. This strain was designated KH10. Single hop experiments with KH10 were performed as described in [8] with modifications for plasmid expression of *rpoH*. For induction of *rpoH* in KH10, overnight cultures were selected for Tet and subsequently grown in LB absent for Tet. 1 hour prior to temperature shift for induction of Mu transposition, aTc was added. Genomic DNA was extracted with Wizards Genomic DNA Kit, and

sequencing was performed by Novogene on NovaSeq PE150 platform. Partitioning of the genome into 100 bins was described previously [8]. Data was processed using custom script described in [8] without LASSO regression for normalization. Instead, the number of insertions per bin was first corrected for total number of read counts, followed by correcting for replication effect by normalizing to the total number of *E. coli* reads mapped to that bin. The average of three biological replicates and standard deviation was used to plot data for normalized transposition frequency.

References

1. Gonzalez JM, Aranda B. Microbial Growth under Limiting Conditions-Future Perspectives. Microorganisms. 2023;11. doi:10.3390/microorganisms11071641

2. Bremer H, Dennis PP. Modulation of Chemical Composition and Other Parameters of the Cell at Different Exponential Growth Rates. EcoSal Plus. 2008;3. doi:10.1128/ecosal.5.2.3

3. Klappenbach JA, Dunbar JM, Schmidt TM. rRNA operon copy number reflects ecological strategies of bacteria. Appl Environ Microbiol. 2000;66: 1328–1333. doi:10.1128/AEM.66.4.1328-1333.2000

4. Fleurier S, Dapa T, Tenaillon O, Condon C, Matic I. rRNA operon multiplicity as a bacterial genome stability insurance policy. Nucleic Acids Res. 2022; 1–20. doi:10.1093/nar/gkac332

5. Condon C, Squires C, Squires CL. Control of rRNA transcription in Escherichia coli. Microbiol Rev. 1995;59: 623–645. doi:10.1128/mr.59.4.623-645.1995

6. Gaal T, Bratton BP, Sanchez-Vazquez P, Sliwicki A, Sliwicki K, Vegel A, et al. Colocalization of distant chromosomal loci in space in *E. Coli*: A bacterial nucleolus. Genes Dev. 2016;30: 2272–2285. doi:10.1101/gad.290312.116

7. Lioy VS, Cournac A, Marbouty M, Duigou S, Mozziconacci J, Espéli O, et al. Multiscale Structuring of the E. coli Chromosome by Nucleoid-Associated and Condensin Proteins. Cell. 2018;172: 771-783.e18. doi:10.1016/j.cell.2017.12.027

8. Walker DM, Freddolino PL, Harshey RM. A Well-Mixed E. coli Genome: Widespread Contacts Revealed by Tracking Mu Transposition. Cell. 2020;180: 703-716.e18. doi:10.1016/j.cell.2020.01.031

9. Walker DM, Harshey RM. Deep sequencing reveals new roles for MuB in transposition immunity and target-capture and redefines the insular Ter region of E. coli. Mob DNA. 2020;11: 26. doi:10.1186/s13100-020-00217-9

10. Mercier R, Petit MA, Schbath S, Robin S, El Karoui M, Boccard F, et al. The MatP/matS Site-Specific System Organizes the Terminus Region of the E. coli Chromosome into a Macrodomain. Cell. 2008;135: 475–485. doi:10.1016/j.cell.2008.08.031

11. Celli J, Tsolis RM. Bacteria, the endoplasmic reticulum and the unfolded protein response: friends or foes? Nat Rev Microbiol. 2015;13: 71–82. doi:10.1038/nrmicro3393

12. Grossman AD, Erickson JW, Gross CA. The *htpR* gene product of *E. coli* is a sigma factor for heat-shock promoters. Cell. 1984;38: 383–390. doi:10.1016/0092-8674(84)90493-8

13. Nonaka G, Blankschien M, Herman C, Gross CA, Rhodius VA. Regulon and promoter analysis of the E. coli heat-shock factor, sigma32, reveals a multifaceted cellular response to heat stress. Genes Dev. 2006;20: 1776–1789. doi:10.1101/gad.1428206

650 14. John J, Jabbar J, Badjatia N, Rossi MJ, Lai WKM, Pugh BF. Genome-wide promoter assembly in E.
651 coli measured at single-base resolution. Genome Res. 2022;32: 878–892.
652 doi:10.1101/gr.276544.121

653 15. Nielsen HJ, Ottesen JR, Youngren B, Austin SJ, Hansen FG. The Escherichia coli chromosome is
654 organized with the left and right chromosome arms in separate cell halves. Mol Microbiol.
655 2006;62: 331–338. doi:10.1111/j.1365-2958.2006.05346.x

656 16. Tosa T, Pizer LI. Biochemical bases for the antimetabolite action of L-serine hydroxamate. J
657 Bacteriol. 1971;106: 972–982. doi:10.1128/jb.106.3.972-982.1971

658 17. Gourse RL, Chen AY, Gopalkrishnan S, Sanchez-Vazquez P, Myers A, Ross W. Transcriptional
659 Responses to ppGpp and DksA. Annu Rev Microbiol. 2018;72: 163–184. doi:10.1146/annurev-
660 micro-090817-062444

661 18. Zhang Y, Gross CA. Cold Shock Response in Bacteria. Annu Rev Genet. 2021;55: 377–400.
662 doi:10.1146/annurev-genet-071819-031654

663 19. Cao H, Wei D, Yang Y, Shang Y, Li G, Zhou Y, et al. Systems-level understanding of ethanol-
664 induced stresses and adaptation in E. coli. Sci Rep. 2017;7: 44150. doi:10.1038/srep44150

665 20. Macvanin M, Edgar R, Cui F, Trostel A, Zhurkin V, Adhya S. Noncoding rnas Binding to the
666 Nucleoid Protein HU in Escherichia coli. J Bacteriol. 2012;194: 6046–6055. doi:10.1128/JB.00961-
667 12

668 21. Ladouceur AM, Parmar BS, Biedzinski S, Wall J, Tope SG, Cohn D, et al. Clusters of bacterial RNA
669 polymerase are biomolecular condensates that assemble through liquid-liquid phase separation.
670 Proceedings of the National Academy of Sciences. 2020;117: 18540–18549.
671 doi:10.1073/pnas.2005019117

672 22. Cui L, Vigouroux A, Rousset F, Varet H, Khanna V, Bikard D. A CRISPRi screen in E. coli reveals
673 sequence-specific toxicity of dCas9. Nat Commun. 2018;9: 1912. doi:10.1038/s41467-018-04209-
674 5

675 23. Lee C, Cox RM, Papoulas O, Horani A, Drew K, Devitt CC, et al. Functional partitioning of a liquid-
676 like organelle during assembly of axonemal dyneins. Carter AP, Akhmanova A, Stearns T, Kikkawa
677 M, editors. Elife. 2020;9: e58662. doi:10.7554/eLife.58662

678 24. Yang D, Ye X, Lorimer GH. Symmetric GroEL: GroES2 complexes are the protein-folding functional
679 form of the chaperonin nanomachine. Proceedings of the National Academy of Sciences.
680 2013;110. doi:10.1073/pnas.1318862110

681 25. Fayet O, Ziegelhoffer T, Georgopoulos C. The groES and groEL heat shock gene products of
682 Escherichia coli are essential for bacterial growth at all temperatures. J Bacteriol. 1989;171:
683 1379–1385. doi:10.1128/jb.171.3.1379-1385.1989

684 26. Cowing DW, Bardwellt JCA, Craigt EA, Woolfordt C, Hendrix RW, Gross CA. Consensus sequence
685 for Escherichia coli heat shock gene promoters. Proceedings of the National Academy of
686 Sciences. 1985;82. doi: 10.1073/pnas.82.9.2679

687 27. Guisbert E, Herman C, Lu CZ, Gross CA. A chaperone network controls the heat shock response in
688 E. coli. Genes Dev. 2004;18: 2812–2821. doi:10.1101/gad.1219204

689 28. Lim B, Miyazaki R, Neher S, Siegele DA, Ito K, Walter P, et al. Heat shock transcription factor σ^{32}
690 co-opts the signal recognition particle to regulate protein homeostasis in E. coli. PLoS Biol.
691 2013;11: e1001735. doi:10.1371/journal.pbio.1001735

692 29. Yura T, Guisbert E, Poritz M, Lu CZ, Campbell E, Gross CA. Analysis of σ^{32} mutants defective in
693 chaperone-mediated feedback control reveals unexpected complexity of the heat shock
694 response. Proceedings of the National Academy of Sciences. 2007;104: 17638–17643.
695 doi:10.1073/pnas.0708819104

696 30. Maeda H, Fujita N, Ishihama A. Competition among seven Escherichia coli σ subunits: relative
697 binding affinities to the core RNA polymerase. Nucleic Acids Res. 2000;28: 3497–3503.
698 doi:10.1093/nar/28.18.3497

699 31. Ishihama A. Functional Modulation of Escherichia Coli RNA Polymerase. Annu Rev Microbiol.
700 2000;54: 499–518. doi:10.1146/annurev.micro.54.1.499

701 32. Joo DM, Nolte A, Calendar R, Zhou YN, Jin DJ. Multiple regions on the Escherichia coli heat shock
702 transcription factor sigma32 determine core RNA polymerase binding specificity. J Bacteriol.
703 1998;180: 1095–1102. doi:10.1128/JB.180.5.1095-1102.1998

704 33. Harshey R. M. (2014). Transposable Phage Mu. *Microbiology spectrum*, *2*(5),
705 10.1128/microbiolspec.MDNA3-0007-2014. https://doi.org/10.1128/microbiolspec.MDNA3-
706 0007-2014

707 34. Belton J-M, McCord RP, Gibcus JH, Naumova N, Zhan Y, Dekker J. Hi-C: a comprehensive
708 technique to capture the conformation of genomes. Methods. 2012;58: 268–276.
709 doi:10.1016/j.ymeth.2012.05.001

710 35. Mcstay B. The p-Arms of Human Acrocentric Chromosomes Play by a Different Set of Rules.
711 Annual Review of Genomics and Human Genetics Annu Rev Genom Hum Genet 2023. 2024;24:
712 48. doi:10.1146/annurev-genom-101122

713 36. Sochorová, J., Gálvez, F., Matyášek, R., Garcia, S., & Kovařík, A. (2021). Analyses of the Updated
714 "Animal rDNA Loci Database" with an Emphasis on Its New Features. *International journal of*
715 *molecular sciences*, *22*(21), 11403. https://doi.org/10.3390/ijms222111403

716 37. Tsuneaki A, Ciarán C, Justina V, Dmitry Z, Binghua S, Michaal A-O, et al. Construction and Initial
717 Characterization of Escherichia coli Strains with Few or No Intact Chromosomal rRNA Operons. J
718 Bacteriol. 1999;181: 3803–3809. doi:10.1128/jb.181.12.3803-3809.1999

719 38. Campbell, E. A., Korzheva, N., Mustaev, A., Murakami, K., Nair, S., Goldfarb, A., & Darst, S. A.
720 (2001). Structural mechanism for rifampicin inhibition of bacterial rna polymerase. *Cell*, *104*(6),
721 901–912. https://doi.org/10.1016/s0092-8674(01)00286-0

722 39. Dash S, Lamb MC, Lange JJ, McKinney MC, Tsuchiya D, Guo F, et al. rRNA transcription is integral
723 to phase separation and maintenance of nucleolar structure. PLoS Genet. 2023;19.
724 doi:10.1371/journal.pgen.1010854

725 40. Enz S, Braun V, Crosa JH. Transcription of the region encoding the ferric dicitrate-transport
726 system in Escherichia coli: similarity between promoters for fecA and for extracytoplasmic
727 function sigma factors. Gene. 1995;163: 13–18. doi:10.1016/0378-1119(95)00380-o

728 41. Enz S, Mahren S, Stroeher UH, Braun V. Surface signaling in ferric citrate transport gene
729 induction: interaction of the FecA, FecR, and FecI regulatory proteins. J Bacteriol. 2000;182: 637–
730 646. doi:10.1128/JB.182.3.637-646.2000

731 42. Ferguson AD, Chakraborty R, Smith BS, Esser L, van der Helm D, Deisenhofer J. Structural Basis of
732 Gating by the Outer Membrane Transporter FecA. Science (1979). 2002;295: 1715–1719.
733 doi:10.1126/science.1067313

734 43. Susanne M, Volkmar B. The FecI Extracytoplasmic-Function Sigma Factor of Escherichia coli
735 Interacts with the β′ Subunit of RNA Polymerase. J Bacteriol. 2003;185: 1796–1802.
736 doi:10.1128/jb.185.6.1796-1802.2003

737 44. Erickson JW, Gross CA. Identification of the sigma E subunit of Escherichia coli RNA polymerase:
738 a second alternate sigma factor involved in high-temperature gene expression. Genes Dev.
739 1989;3: 1462–1471. doi:10.1101/gad.3.9.1462

740 45. Missiakas D, Raina S. The extracytoplasmic function sigma factors: role and regulation. Mol
741 Microbiol. 1998;28: 1059–1066. doi:10.1046/j.1365-2958.1998.00865.x

742 46. Missiakas D, Mayer MP, Lemaire M, Georgopoulos C, Raina S. Modulation of the Escherichia coli
743 σ^E (RpoE) heat-shock transcription-factor activity by the RseA, RseB and RseC proteins. Mol
744 Microbiol. 1997;24: 355–371. doi:https://doi.org/10.1046/j.1365-2958.1997.3601713.x

745 47. Campbell EA, Tupy JL, Gruber TM, Wang S, Sharp MM, Gross CA, et al. Crystal Structure of
746 Escherichia coli σE with the Cytoplasmic Domain of Its Anti-σ RseA. Mol Cell. 2003;11: 1067–
747 1078. doi:https://doi.org/10.1016/S1097-2765(03)00148-5

748 48. Kanehara K, Ito K, Akiyama Y. YaeL proteolysis of RseA is controlled by the PDZ domain of YaeL
749 and a Gln-rich region of RseA. EMBO J. 2003;22: 6389–6398.
750 doi:https://doi.org/10.1093/emboj/cdg602

751 49. Ades SE, Connolly LE, Alba BM, Gross CA. The Escherichia coli sigma(E)-dependent
752 extracytoplasmic stress response is controlled by the regulated proteolysis of an anti-sigma
753 factor. Genes Dev. 1999;13: 2449–2461. doi:10.1101/gad.13.18.2449

754 50. Mathew R, Chatterji D. The evolving story of the omega subunit of bacterial RNA polymerase.
755 Trends in Microbiology. 2006. pp. 450–455. doi:10.1016/j.tim.2006.08.002

756 51. Ross W, Gosink KK, Salomon J, Igarashi K, Zou C, Ishihama A, et al. A Third Recognition Element in
757 Bacterial Promoters: DNA Binding by the α Subunit of RNA Polymerase. Science (1979). 1993;262:
758 1407–1413. doi:10.1126/science.8248780

759 52. Ziemienowicz, A., Skowyra, D., Zeilstra-Ryalls, J., Fayet, O., Georgopoulos, C., & Zylicz, M. (1993).
760 Both the Escherichia coli chaperone systems, GroEL/GroES and DnaK/DnaJ/GrpE, can reactivate
761 heat-treated RNA polymerase. Different mechanisms for the same activity. *The Journal of*
762 *biological chemistry*, *268*(34), 25425–25431.

763 53. Cabrera JE, Jin DJ. The distribution of RNA polymerase in Escherichia coli is dynamic and
764 sensitive to environmental cues. Mol Microbiol. 2003;50: 1493–1505. doi:10.1046/j.1365-
765 2958.2003.03805.x

766 54. Stracy M, Lesterlin C, Garza de Leon F, Uphoff S, Zawadzki P, Kapanidis AN. Live-cell
767 superresolution microscopy reveals the organization of RNA polymerase in the bacterial nucleoid.
768 Proc Natl Acad Sci U S A. 2015/07/29. 2015;112: E4390–E4399. doi:10.1073/pnas.1507592112

769 55. Jin DJ, Cagliero C, Zhou YN. Growth rate regulation in Escherichia coli. FEMS Microbiol Rev.
770 2012;36: 269–287. doi:10.1111/j.1574-6976.2011.00279.x

771 56. Weng X, Bohrer CH, Bettridge K, Lagda AC, Cagliero C, Jin DJ, et al. Spatial organization of RNA
772 polymerase and its relationship with transcription in Escherichia coli. Proceedings of the National
773 Academy of Sciences. 2019;116: 20115–20123. doi:10.1073/pnas.1903968116

774 57. Gibson DG, Young L, Chuang R-Y, Venter JC, Hutchison CA, Smith HO. Enzymatic assembly of DNA
775 molecules up to several hundred kilobases. Nat Methods. 2009;6: 343–345.
776 doi:10.1038/nmeth.1318

777 58. Datsenko KA, Wanner BL. One-step inactivation of chromosomal genes in *Escherichia coli* K-12
778 using PCR products. Proceedings of the National Academy of Sciences. 2000;97: 6640–6645.
779 doi:10.1073/pnas.120163297

780

Supporting Information

S1 Fig. Distribution of *rrn* operons on the *E. coli* genome. On the circular *E. coli* chromosome, replication originates at *oriC*, with two bidirectional replication forks traversing each arm (replicore), terminating within the Ter region. Locations of the *rrn* operons shown to cluster by two different methodologies (see main text) are indicated by blue-filled circles. Positions of the operons on the circular chromosome are not drawn to scale. Organization of a typical *rrn* operon is shown for *rrnG,* with tRNAGlu2 between 16S and 23S; some *rrn* loci possess distal tRNAs. P1 and P2 promoters are indicated by forward arrows.

S2 Fig. Microscopy of cells labeled with *parS*-ParB at *rrnA* and *rrnD*. (A) Insets of a complete field of cells (phase contrast and fluorescence) shown in B. *rrnA* and *rrnD* were tagged with GFP-ParB and CFP-ParB, respectively, as described in Fig 1A, and processed as described in Fig 1B. (B) Complete field and position of identified foci.

S3 Fig. Effect of Δ*nusB,* Δ*rpoZ,* and Δ*nc5* on the distance between *rrnA* and *rrnD*. Effect of deletions of factors known to participate in RNAP condensate on *rrnA*-*rrnD* distance. Experimental conditions are similar to those in Fig 1.

S4 Fig. Deregulation of GroEL disrupts *rrnA-rrnD* clustering. (A) Scheme for pulldown of proteins in the vicinity of all *rrn* loci. dCas9-FLAG (pink/green) was directed upstream of all 7 *rrn* loci by expressing sgRNA specific for each target. Formaldehyde was used to crosslink dCas9 to putative bridging factor(s) (purple). The dCas9-linked 'complex' was then immunoprecipitated and subjected to mass spectrometry. (B) Significantly enriched proteins in pulldown with gRNA targeting *yeiP* (*rrnC*). Each protein is identified by a circle. Each axis represents the z-score of each protein in separate experiments. Lines from the axes indicate the cut-off for enrichment. Red circles and black circles indicate proteins that fall above and below the False Discovery Rate (FDR) (5%), respectively. Proteins significantly enriched (z score>2.5) are in the top-right square

(red balls with corresponding protein name). See S6 Fig for data obtained for the remaining gRNAs. (C) Distance between *rrnA-D* operons in WT and Δ*groEL* strains expressing either both *groES/groEL* or *groEL* alone from pAraBAD plasmid. Other descriptions as in Fig 1B. (D) Distance between *rrnA-D* in WT and Δ*groEL* strains expressing *groES/groEL* from either pAra or the native *groE* promoter.

S5 Fig. Efficiency of gRNA in cell lethality. gRNAs employed in SFig 4 were assayed for their ability to target chromosomal loci by substituting dCas9 with Cas9 and monitoring resultant cell death. Lethality was determined by the fraction of CFU that survive induction of Cas9 and gRNA compared to the CFU of non-induced control (y-axis). Gene names on the x-axis indicate the targeted gene immediately upstream of the *rrn* operon indicated in parentheses. gRNA targeting *lacZ* without (bolded) and with the protospacer adjacent motif (PAM), were used as negative and positive controls, respectively.

S6 Fig. **Proteins enriched in gRNA pulldowns.** (A-F) Results from gRNAs directed to indicated *rrn* loci. See S4A Fig legend for other experimental details.

S7 Fig. Upset plot of the number of proteins identified in each gRNA pulldown. Aggregated MS results of significantly enriched proteins from dCas9 pulldown. The vertical bar graph on the top shows the number of proteins identified for each individual pull down (black balls). The first seven data points are unique to each sgRNA targeted *rrn*. The horizontal bars indicate the relative protein numbers in each of the unique pull downs. The black lines connecting the other black balls indicate co-occurrence of the proteins in individual pulldowns.

S8 Fig. Growth of Δ*groEL* strain complemented of *groEL* from pAraBAD. Colony morphologies upon induction and repression of GroEL with added arabinose or glucose, respectively, at 30°C (A) and 37°C (B). See S4D Fig and related text.

S9 Fig. RpoH disrupts *rrnA-rrnD* clustering. Representative image of *rrnA-rrnD* foci showing no loss of *rrnA*-GFP foci as seen with heat stress in Fig 1D.

S10 Fig. Effect of heat stress and *rpoH* overexpression on the nucleoid and the distance between non-*rrn* loci. (A) Cell length distribution under heat stress and *rpoH* overexpression. Conditions for heat stress and *rpoH* overexpression are identical to that of Fig 1B and Fig 3A, respectively. 200-300 cells were measured for each sample. Data shown are pooled from three biological replicates. (B) Condensation of the nucleoid under the same conditions as in A, with similar cell numbers and replicates. (C) Conditions tested in A do not affect the distance between *lacZ* and *leuC*. Left, relative position of *lacZ* and *leuC* on the genetic map (not drawn to scale). Right, spatial distance (120nm, 120nm, and 85nm for No Vector, RpoH, and +RpoH, respectively) between *lacZ*-pMT*parS* and *leuC*-P1*parS* as measured by fluorescent microscopy. Conditions for *rpoH* overexpression and induction are identical to that of Fig 3A.

S11 Fig. Morphology of cells over-expressing *rpoH* variants. Phase contrast images of cells carrying the indicated mutation in *rpoH* were grown, imaged, and induced as described in Methods.

S1 Table. Strains and Plasmids used in this study.

S2 Table. Primers Used in this study.

S3 Table. Spectral Data of gRNA targeting *rrnA* pulldown

S4 Table. Spectral Data of gRNA targeting *rrnB* pulldown

S5 Table. Spectral Data of gRNA targeting *rrnG* pulldown

S6 Table. Spectral Data of gRNA targeting *rrnD* pulldown

S7 Table. Spectral Data of gRNA targeting *rrnE* pulldown

S8 Table. Spectral Data of gRNA targeting *rrnH* pulldown

S9 Table. Spectral Data of gRNA targeting *rrnC* pulldown

S Raw Data. Raw Data for figures that contain numerical data. The name on each tab indicates the figure for which the data were used to plot.

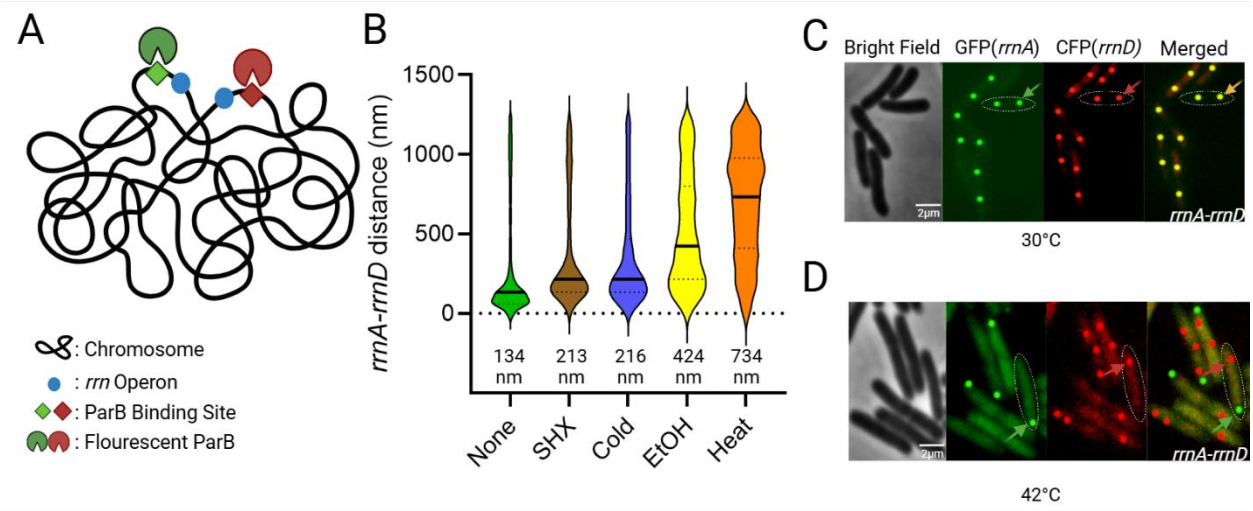
A
: Chromosome
: rrn Operon
: ParB Binding Site
: Flourescent ParB
B
rrnA-rrnD distance (nm)
1500
1000
500
0
134 nm
213 nm
216 nm
424 nm
734 nm
None
SHX
Cold
EtOH
Heat
C
Bright Field
GFP(rrnA)
CFP(rrnD)
Merged
2μm
rrnA-rrnD
30°C
D
2μm
rrnA-rrnD
42°C

856

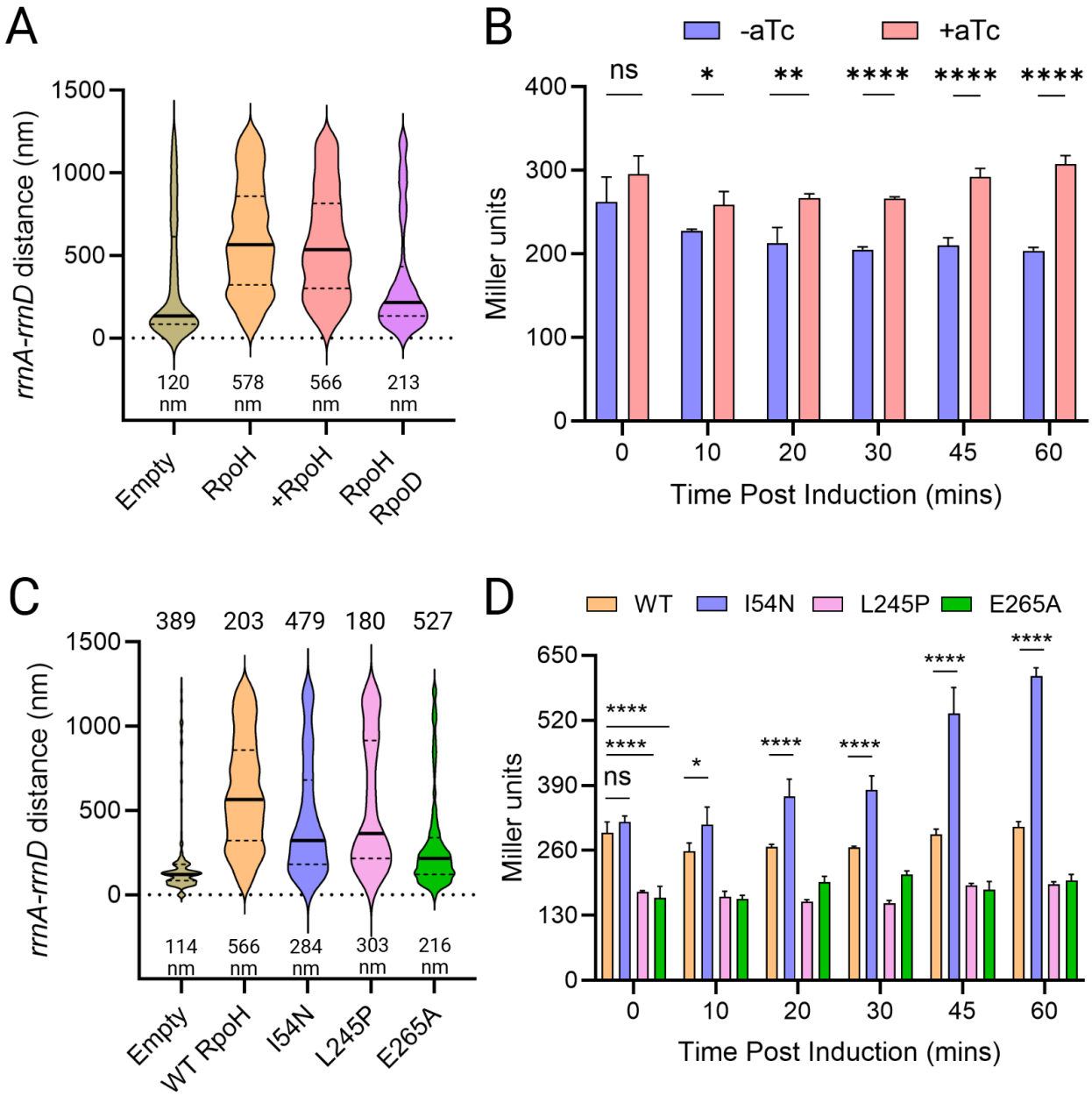
A
rrnA-rrnD distance (nm)
1500
1000
500
0
120 nm
578 nm
566 nm
213 nm
Empty
RpoH
+RpoH
RpoH RpoD
B
-aTc
+aTc
Miller units
400
300
200
100
0
ns
*
**
****
****
****
0
10
20
30
45
60
Time Post Induction (mins)
C
rrnA-rrnD distance (nm)
389
203
479
180
527
1500
1000
500
0
114 nm
566 nm
284 nm
303 nm
216 nm
Empty
WT RpoH
I54N
L245P
E265A
D
WT
I54N
L245P
E265A
Miller units
650
520
390
260
130
0
****
****
ns
*
****
****
****
****
0
10
20
30
45
60
Time Post Induction (mins)

857

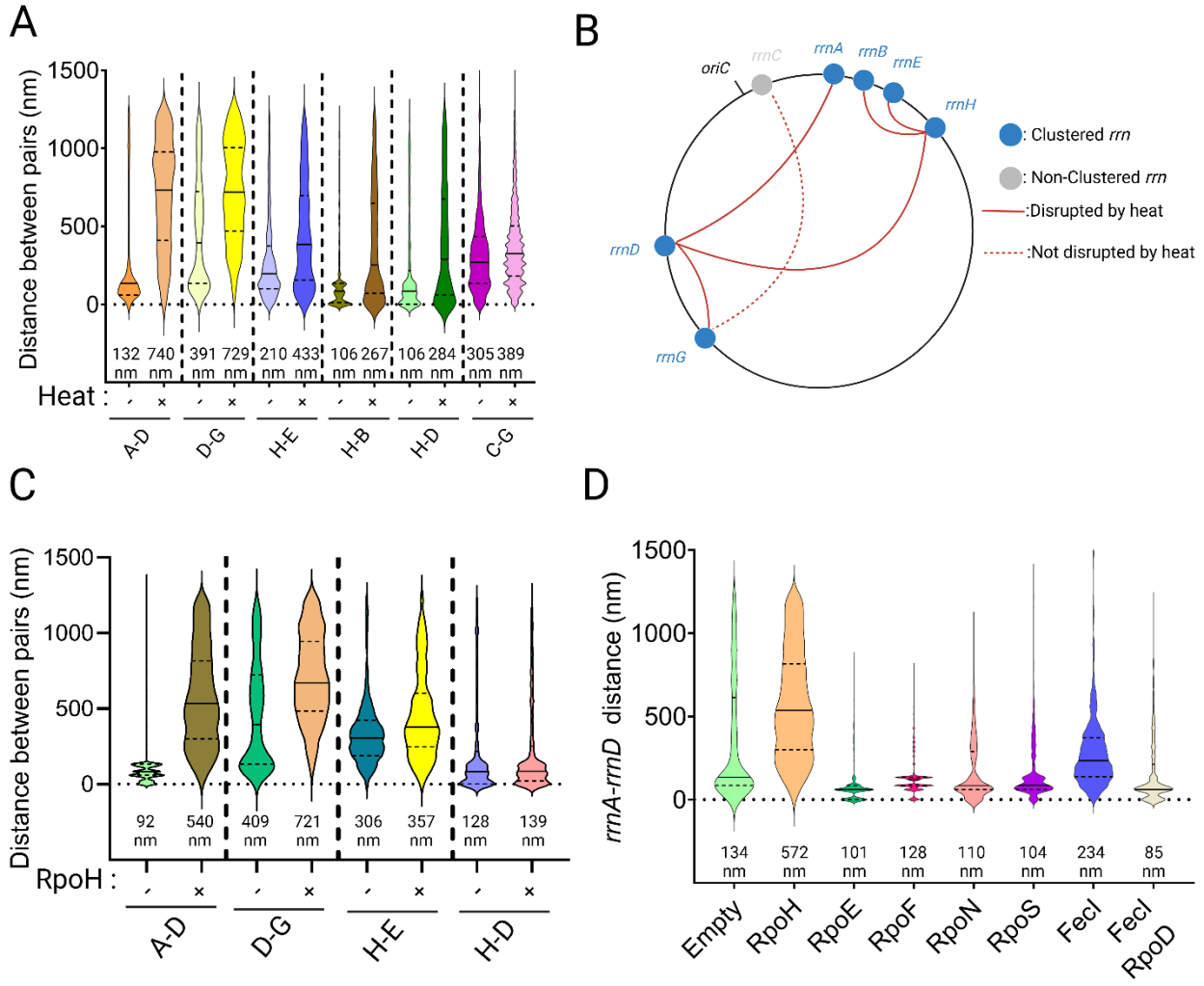
A
Distance between pairs (nm)
1500
1000
500
0
132 nm
740 nm
391 nm
729 nm
210 nm
433 nm
106 nm
267 nm
106 nm
284 nm
305 nm
389 nm
Heat :
A-D
D-G
H-E
H-B
H-D
C-G
B
oriC
rrnC
rrnA
rrnB
rrnE
rrnH
rrnD
rrnG
: Clustered rrn
: Non-Clustered rrn
:Disrupted by heat
:Not disrupted by heat
C
Distance between pairs (nm)
1500
1000
500
0
92 nm
540 nm
409 nm
721 nm
306 nm
357 nm
128 nm
139 nm
RpoH :
A-D
D-G
H-E
H-D
D
rrnA-rrnD distance (nm)
1500
1000
500
0
134 nm
572 nm
101 nm
128 nm
110 nm
104 nm
234 nm
85 nm
Empty
RpoH
RpoE
RpoF
RpoN
RpoS
FecI
FecI RpoD

858

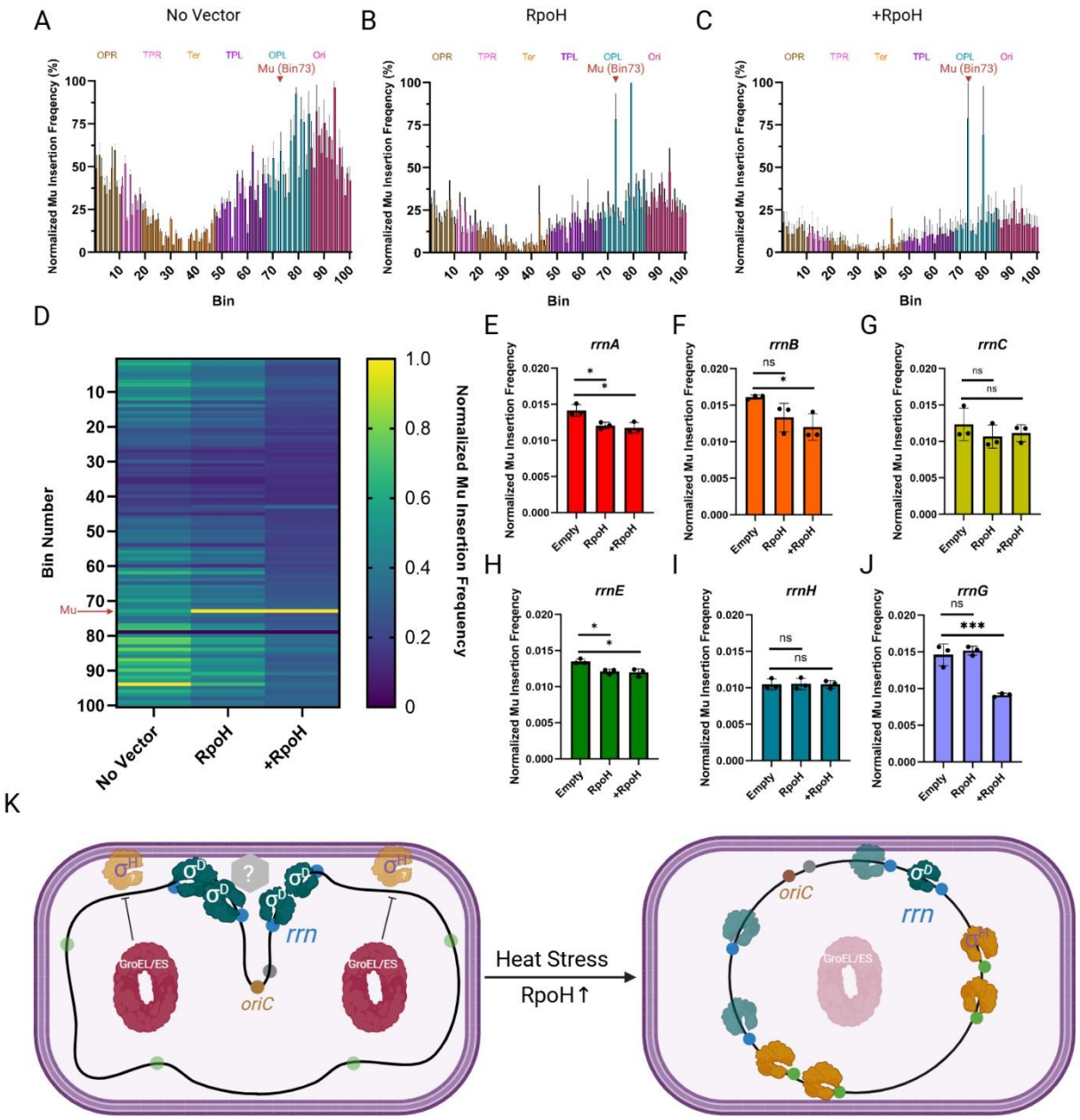
A
No Vector
B
RpoH
C
+RpoH
OPR
TPR
Ter
TPL
OPL
Ori
Mu (Bin73)
Normalized Mu Insertion Freqency (%)
Bin
D
Bin Number
Mu
No Vector
RpoH
+RpoH
Normalized Mu Insertion Frequency
E
rrnA
F
rrnB
G
rrnC
H
rrnE
I
rrnH
J
rrnG
Normalized Mu Insertion Freqency
Empty
RpoH
+RpoH
ns
K
GroEL/ES
rrn
oriC
Heat Stress
RpoH↑

859

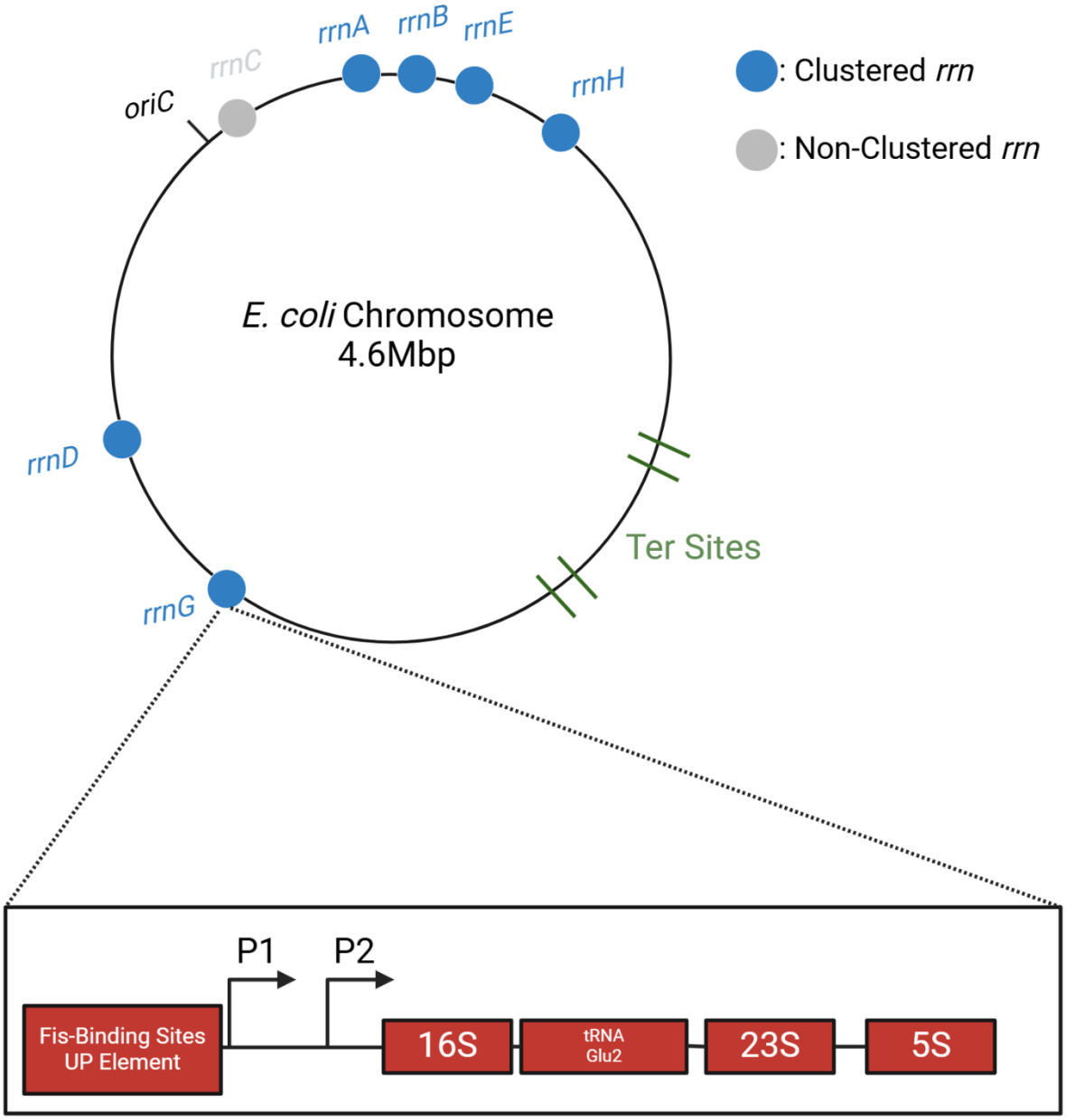
rrnA
rrnB
rrnE
rrnC
rrnH
oriC
: Clustered rrn
: Non-Clustered rrn
E. coli Chromosome
4.6Mbp
rrnD
Ter Sites
rrnG
P1
P2
Fis-Binding Sites
UP Element
16S
tRNA
Glu2
23S
5S

860

861

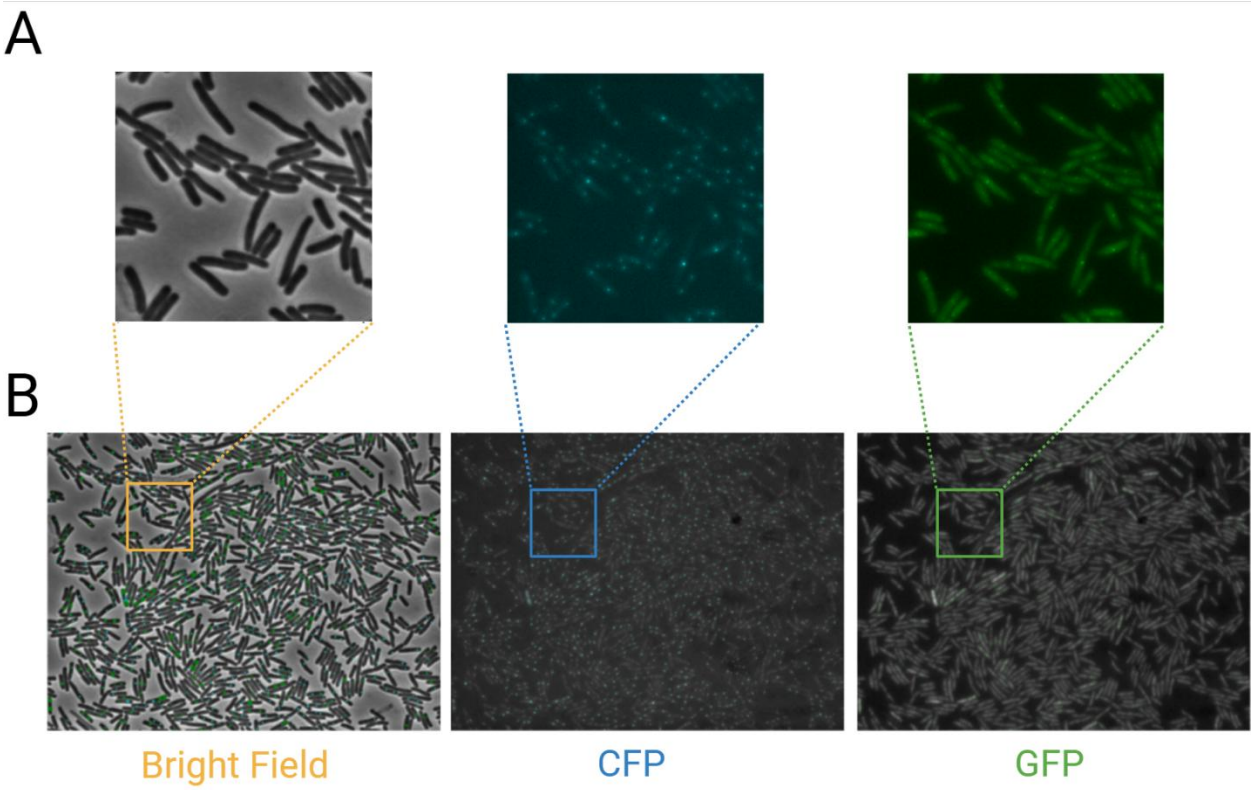
A
B
Bright Field
CFP
GFP

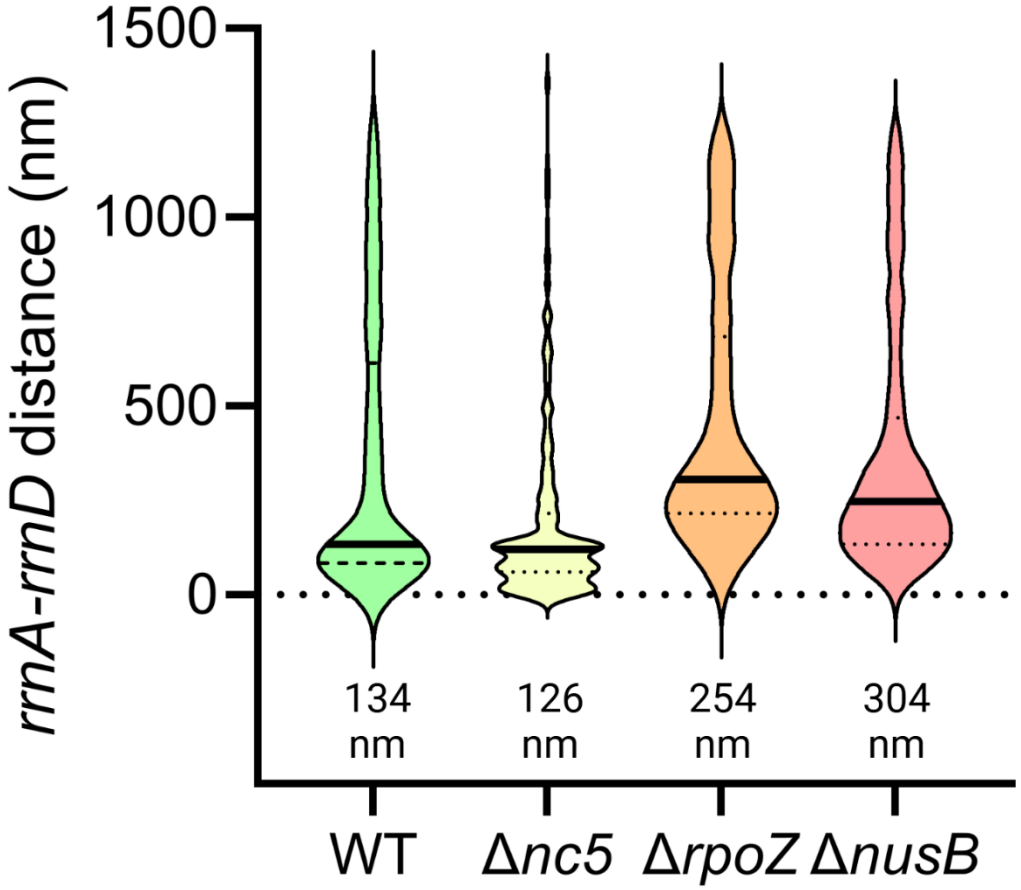
1500
1000
500
0
rrnA-rrnD distance (nm)
134 nm
126 nm
254 nm
304 nm
WT
Δnc5
ΔrpoZ
ΔnusB

864

865

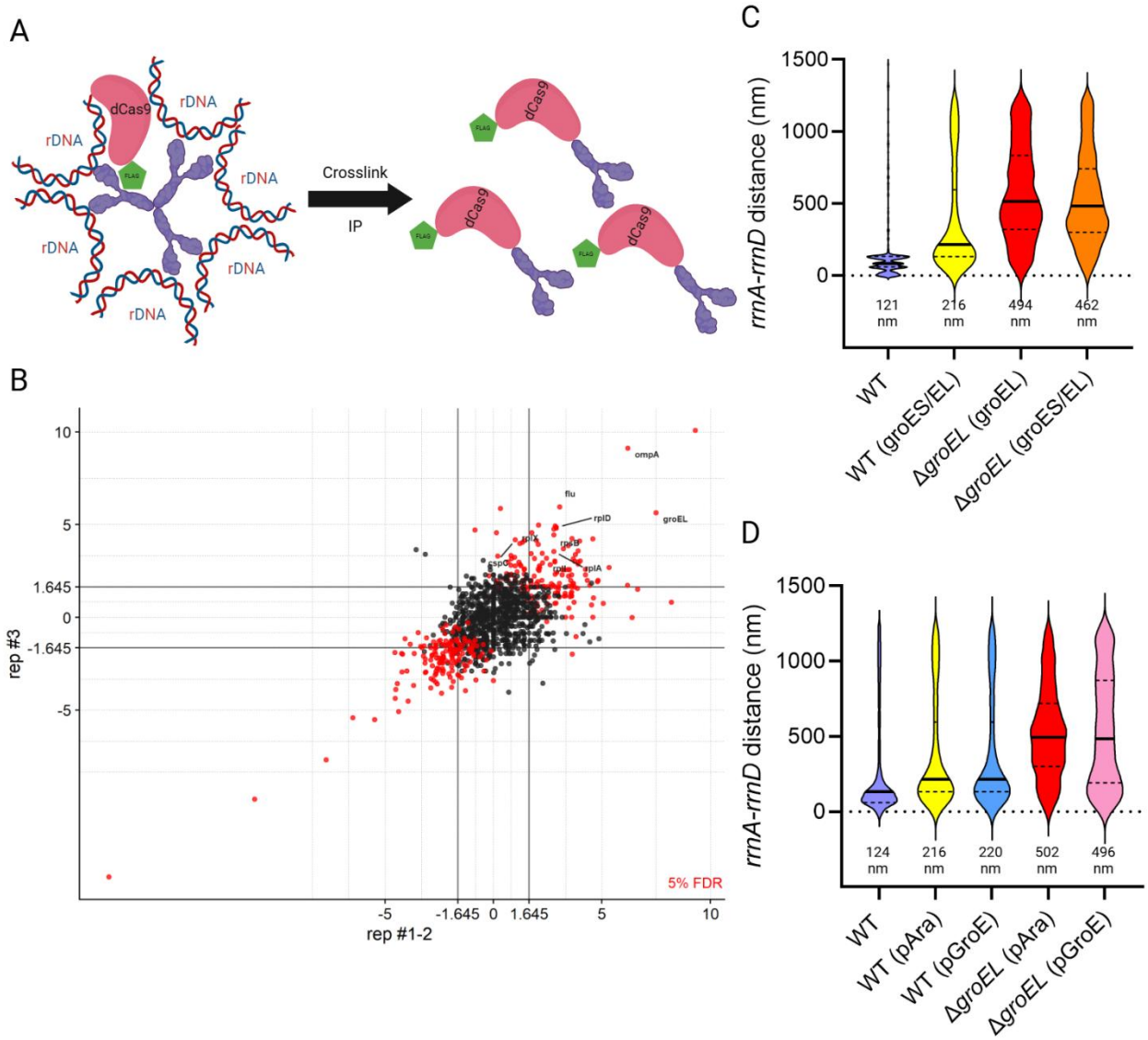
A
dCas9
rDNA
rDNA
rDNA
rDNA
rDNA
rDNA
FLAG
Crosslink
IP
dCas9
dCas9
dCas9
FLAG
B
10
5
1.645
0
-1.645
-5
rep #3
-5
-1.645
0
1.645
5
10
rep #1-2
ompA
flu
rplD
groEL
rplA
5% FDR
C
1500
1000
500
0
rrnA-rrnD distance (nm)
121 nm
216 nm
494 nm
462 nm
WT
WT (groES/EL)
ΔgroEL (groEL)
ΔgroEL (groES/EL)
D
1500
1000
500
0
rrnA-rrnD distance (nm)
124 nm
216 nm
220 nm
502 nm
496 nm
WT
WT (pAra)
WT (pGroE)
ΔgroEL (pAra)
ΔgroEL (pGroE)

866

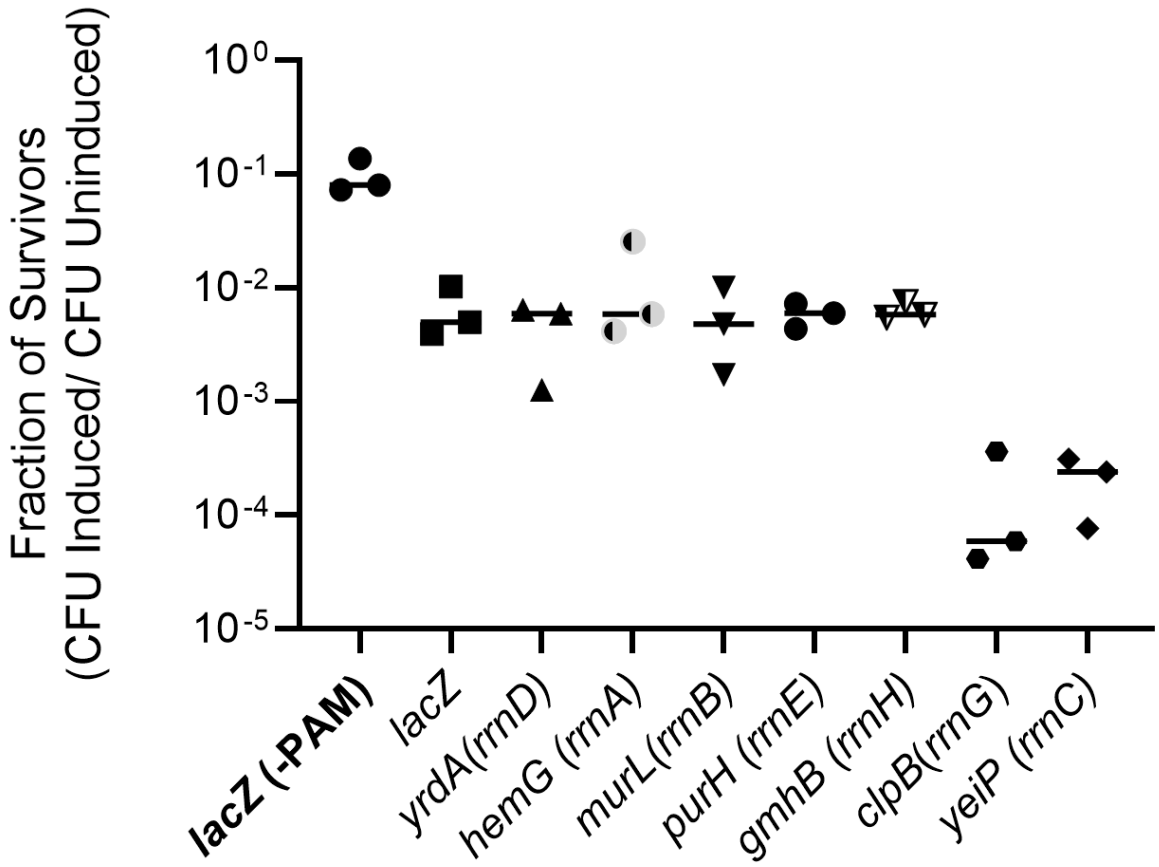
Fraction of Survivors
(CFU Induced/ CFU Uninduced)
10^0
10^-1
10^-2
10^-3
10^-4
10^-5
lacZ (-PAM)
lacZ
yrdA(rrnD)
hemG (rrnA)
murL(rrnB)
purH (rrnE)
gmhB (rrnH)
clpB(rrnG)
yeiP (rrnC)

867

868

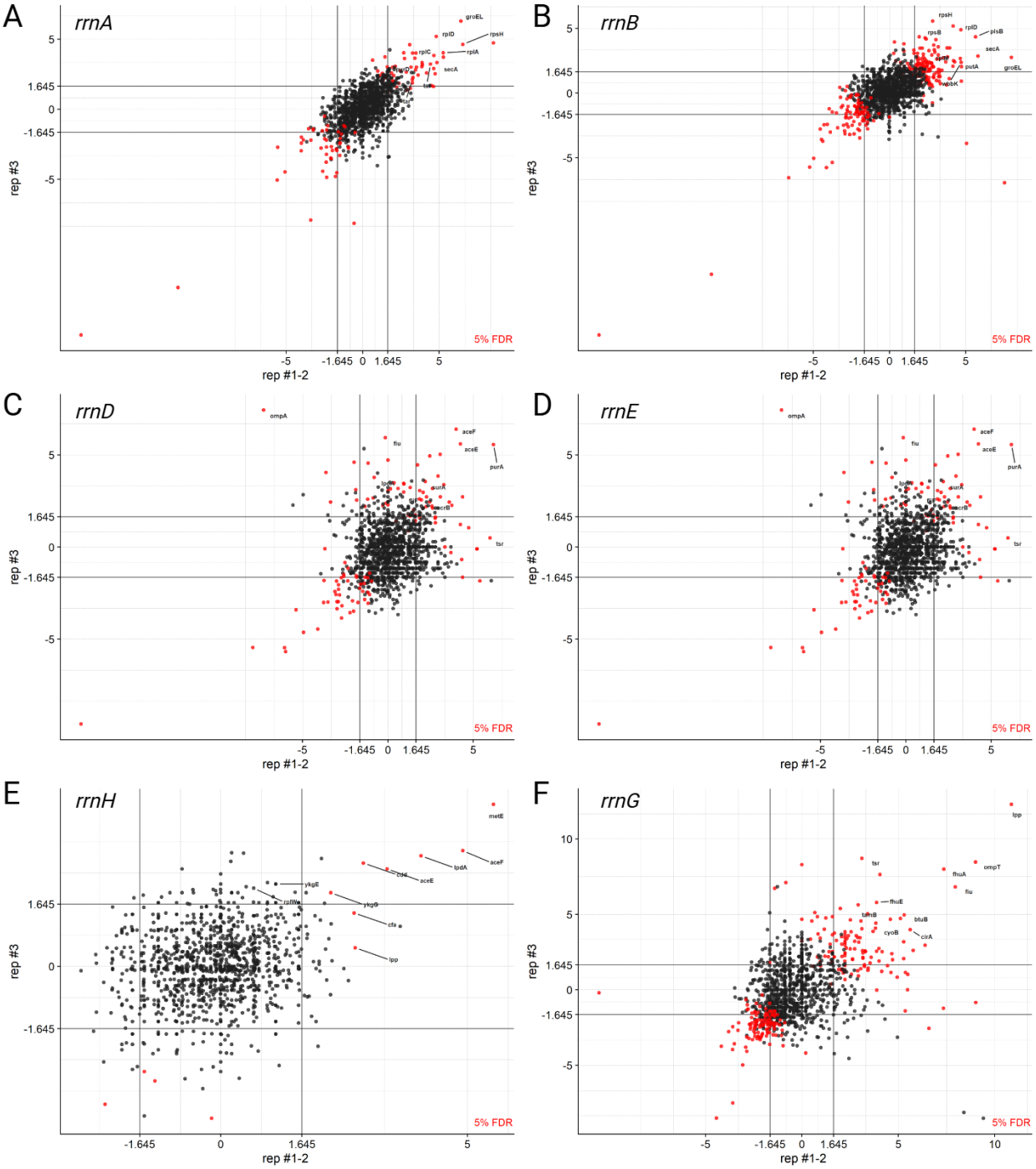
A
rrnA
groEL
rplD
rpsH
rplC
rplA
secA
tsr
5% FDR
rep #3
rep #1-2
B
rrnB
rpsH
rplD
rpsB
plsB
secA
putA
groEL
5% FDR
C
rrnD
ompA
aceF
aceE
purA
fiu
tsr
5% FDR
D
rrnE
ompA
aceF
aceE
purA
fiu
tsr
5% FDR
E
rrnH
metE
aceF
lpdA
aceE
ykgE
ykgG
cfa
lpp
5% FDR
F
rrnG
lpp
tsr
ompT
fhuA
fiu
fhuE
btuB
cyoB
cirA
5% FDR

869

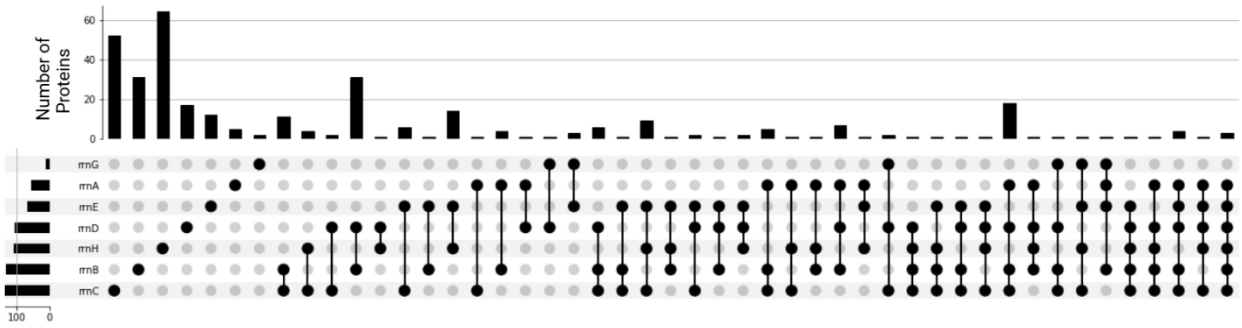
Number of Proteins
60
40
20
0
πnG
πnA
πnE
πnD
πnH
πnB
πnC
100
0

A

30°C

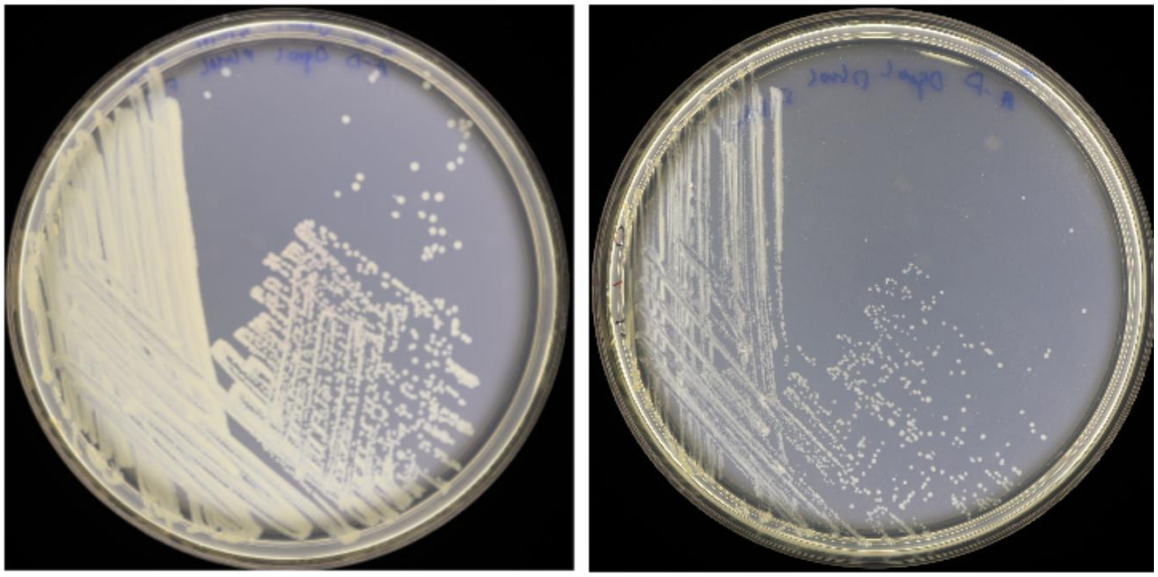

Arabinose Glucose

B

37°C

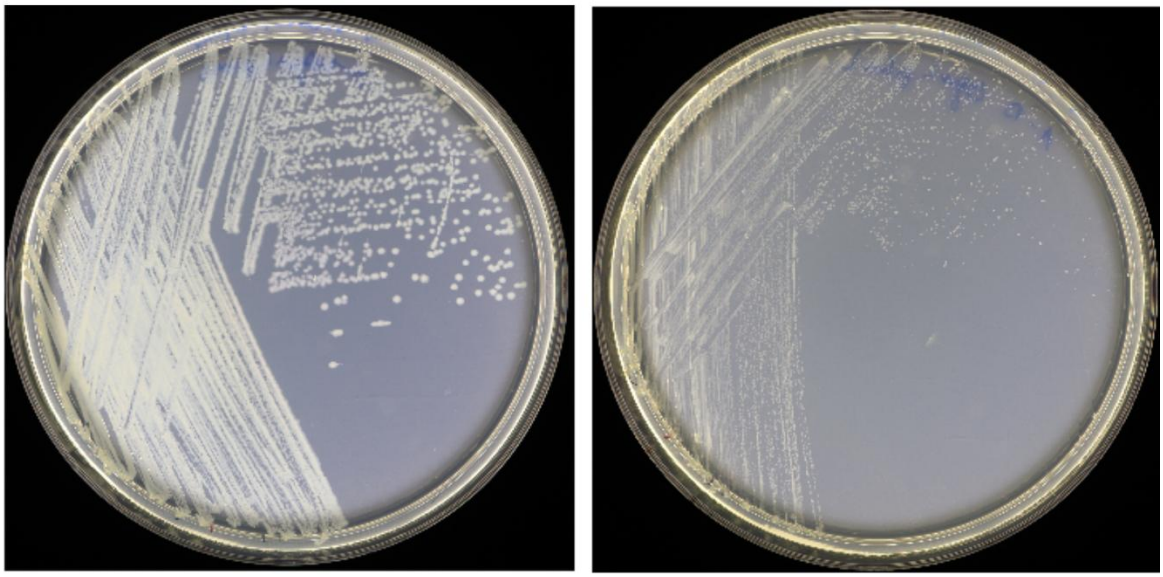

Arabinose Glucose

871

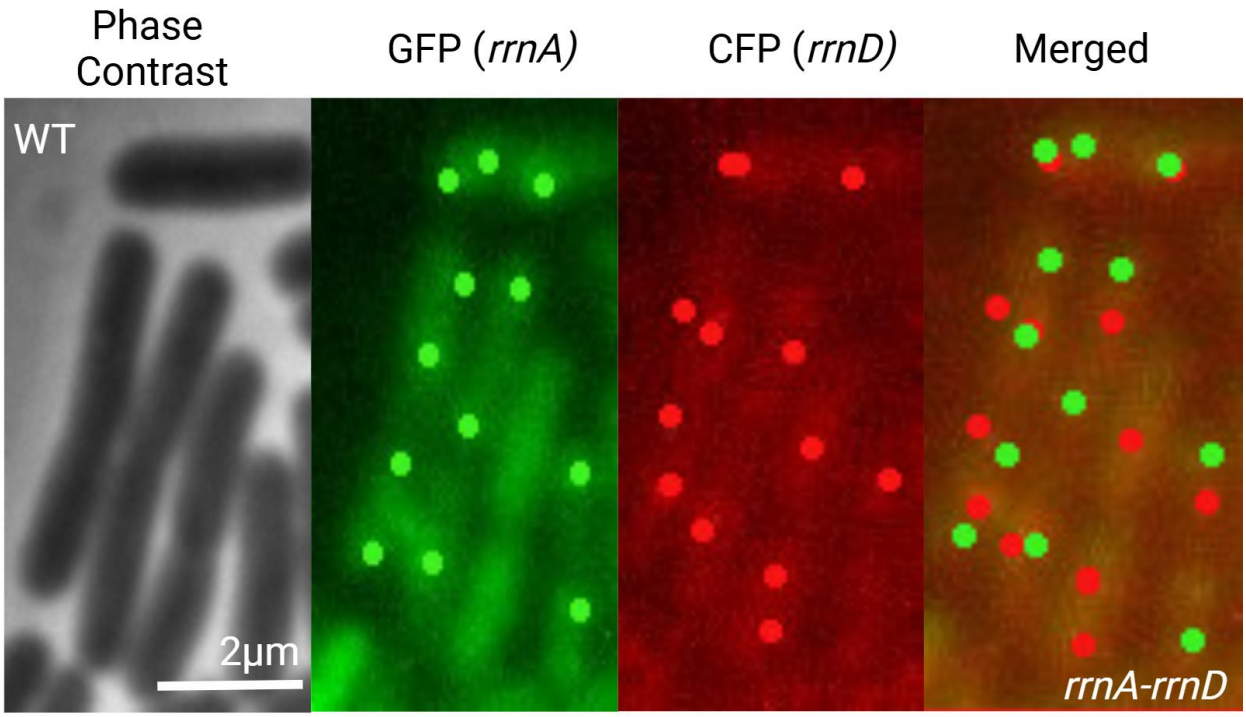

rpoH

872

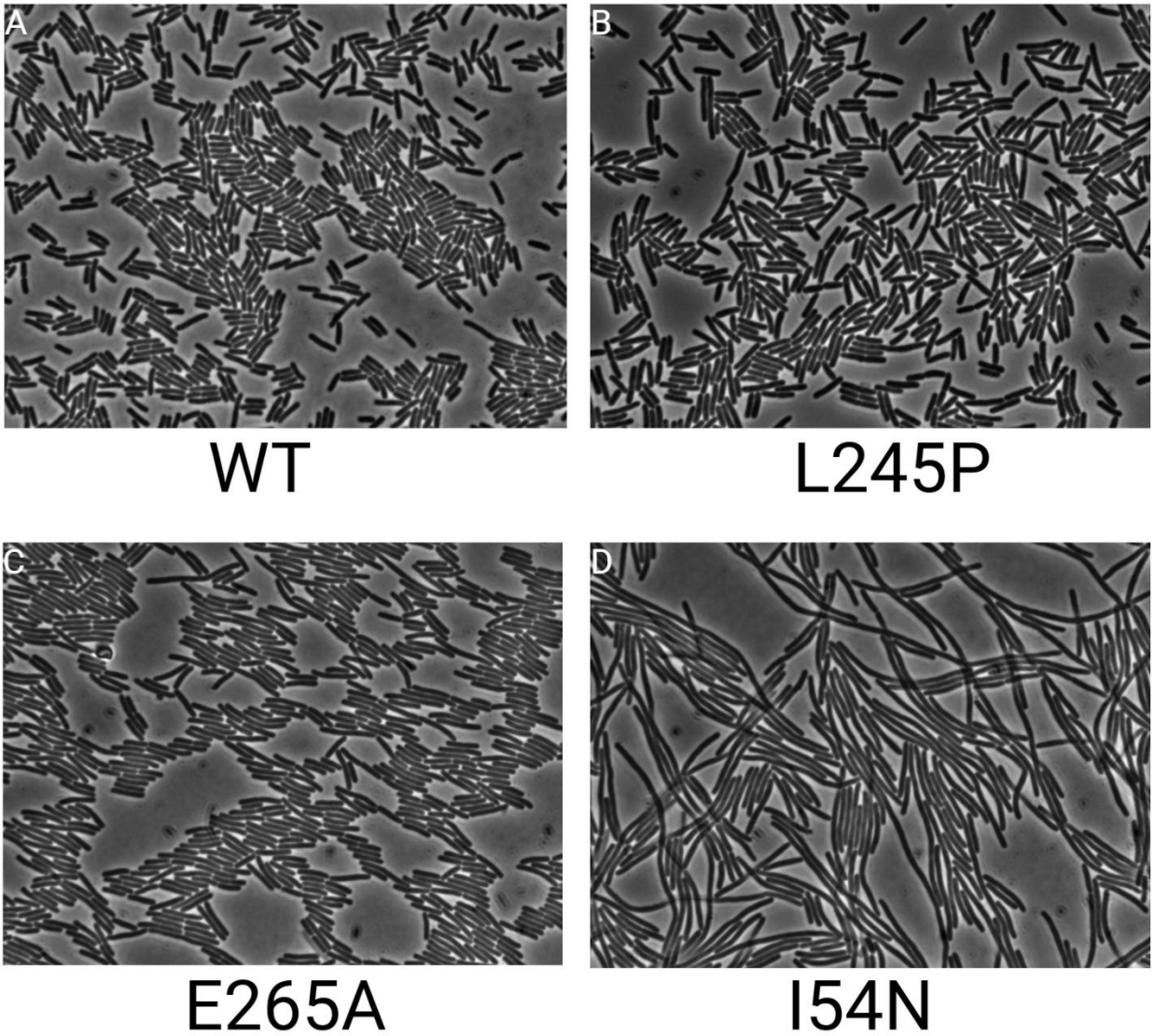

873

Strain		
Strain Name	Genotype or Description	Source
MG1655	Wild-type for all insertion of *parS* seqeuences	Lab Collection
HM8305	Lysogen of Mucts62	Lab Collection
CW45	Mucts62::CamR lysogen. Cam cassette is inserted at position 35040	Lab Collection
BW25141	Host for R6K-origin plasmids	Gift of Ian Molineux
KH2	MG1655Δ*attB*::FRT	This Work
KH3	MG1655 *yrdA*::P1-*parS*(*rrnD*) *hemG*::pMT-parS (*rrnA)*	This Work
KH4	MG1655 *yrdA*::P1-*parS*(*rrnD*) *clpB*::pMT-parS (*rrnG)*	This Work
KH5	MG1655 *gmhB*::P1-*parS*(*rrnH*) *purH*::pMT-parS (*rrnE)*	This Work
KH6	MG1655 *gmhB*::P1-*parS*(*rrnH*) *murI*::pMT-parS (*rrnB)*	This Work
KH7	MG1655 *gmhB*::P1-*parS*(*rrnH*) *yrdA*::pMT-parS (*rrnD)*	This Work
KH8	MG1655 yeiP::P1-*parS*(*rrnC*) *clpB*::pMT-parS (*rrnC)*	This Work
KH9	MG1655Δ*groEL* pKH14	This Work
KH10	KH2 mlaF::KanR-Mucts62::Cam^r	This Work
KH11	MG1655 Δ*nusB*::Kan^r	This Work
KH12	MG1655 Δ*rpoZ*::Kan^r	This Work
KH13	MG1655 Δ*nc5*::Kan^r	This Work
Plasmids		
Name	Description	Source
pKD46	pSC101 derivative, Source of λred proteins, repA101ts	Lab Collection
pKD3	R6K origin, Cam^r	Lab Collection
pKD4	R6K origin, Kan^r	Lab Collection
pCP20	Temperative Sensitive Origin, Source of Flp Recombinase	Lab Collection
pFHC2973	pBR322 origin, provide P1 ParB-GFP, pMT-ParB-CFP fusion	Lab Collection [1]

pCT3110	Source of dcas9-3X FLAG	[2]
pMAZ-SK CR 2.0	Source of Cas9 under control of pTet	[3]
pMAZ-SK sfgfp	Destination Vector for Golden Gate assembly of gRNA	Gift of Kamyab Javanmardi
pBAD33-Flp	Flp Recombinase Under control of pAraBAD	Gift of Chien Hui Ma
pSC101	Low copy vector, Source of pTet-TetA	Lab Collection
pKH2	pBAD33 derivative, pAraBAD-λInt, AmpR	This Work
pKH3	pKD3 derivative, P1-*parS* linked to Cam cassette	This Work
pKH4	pKD4 derivative, pMT-*parS* linked to Kan cassette	This Work
pKH5	Derivative of pCT3110, dcas9-3XFLAG under control of pAraBAD, AmpR	This Work
pKH6	pMAZ-SK sfgfp derivative, gRNA targeting *rrnA* ,KanR	This Work
pKH7	pMAZ-SK sfgfp derivative, gRNA targeting *rrnD*,KanR	This Work
pKH8	pMAZ-SK sfgfp derivative, gRNA targeting *rrnC* ,KanR	This Work
pKH9	pMAZ-SK sfgfp derivative, gRNA targeting *rrnB* ,KanR	This Work
pKH10	pMAZ-SK sfgfp derivative, gRNA targeting *rrnH* ,KanR	This Work
pKH11	pMAZ-SK sfgfp derivative, gRNA targeting *rrnG* ,KanR	This Work
pKH12	pMAZ-SK sfgfp derivative, gRNA targeting *rrnE* ,KanR	This Work
pKH13	pBAD33 derivative, pAraBAD-GroEL/GroES, CamR	This Work
pKH14	pBAD33 derivative, pAraBAD-GroEL, KanR	This Work
pKH15	pBAD33 derivative, pgroE-GroEL, CamR	This Work
pKH16	pBAD33 derivative, pTetA-*rpoH, KanR*	This Work
pKH17	pBAD33 derivative, pTetA-*rpoH* I54N, KanR	This Work
pKH18	pBAD33 derivative, pTetA-*rpoH* L245P, KanR	This Work
pKH19	pSC101 derivative, p*htpG-lacZ*, CamR	This Work
pKH20	pBAD33 derivative, pTetA-*rpoH* E265A, KanR	This Work
pKH21	pBAD33 derivative, pTetA-*rpoH* pTetR-*tetR-rpoD*, KanR	This Work

pKH22	pKD4 derivative, *attB-sacB* linked to Kan cassette, KanR	This Work
pKH23	pKD4 derivative, attP linked to Kan cassette, KanR	Lab Collection
pKH24	pBAD33 derivative, pTetA-fecI, KanR	This Work
pKH25	pBAD33 derivative, pTetA-*rpoN*, KanR	This Work
pKH26	pBAD33 derivative, pTetA-*rpoS*, KanR	This Work
pKH27	pBAD33 derivative, pTetA-*fliA*, KanR	This Work
pKH28	pBAD33 derivative, pTetA-*rpoE*, KanR	This Work
pKH29	pKH19 derivative, pTetA-*fecI*, pTetR-t*etR-rpoD*	This Work

Table S1. Strains and Plasmids used in this study.

Name	Sequence	Note
KH882	CAAGCTTGCATGCAGATTGCAGCATTACACGTTACTCAATTTACTCTTCCTTAAACACAA	Used with 883 to generate P1 ParS insert
KH883	GCAGCTCCAGCCTACACAATCGCTCAAGACCGAAGCCTTAAACTTTCGCCAT	
KH884	GTCTTGAGCGATTGTGTAGGCTGGA	Used with 885 to generate P1 ParS backbone (pKD3)
KH885	GTGTAATGCTGCAATCTGCATGCAA	
KH888	CCAGTGCCAAGCTTGCATGCAGATTGCAGCGCTGGTGGGGATAAGGATGC	Used with 889 to generate pMT ParS insert
KH889	CAGCCTACACAATCGCTCAAGACGTGTAATGCGAAATTATGAGTCACGAAGAGGT	
KH890	ATTACACGTCTTGAGCGATTGTGT	Used with 889 to generate pMT ParS backbone (pKD4)
KH891	GCTGCAATCTGCATGCAAGCT	
KH955	GGAGCACGCACCAATATCCAGGATGGCAGTTTGCATGCAGATTGCAGCATTAC	Used with 956 to insert P1-parS at *yrdA* (rrnD)
KH956	GGGTTGTACGAGGATTTATGAGTGACATGCAACATGCCATGGTCCATATGAATATCCTCC	
KH1140	ATGTACATTATGTACAGATCGGAGCACGCACCAATATCCTTGCATGCAGATTGCAGCAGG	Used with 1141 to insert pMT-parS at *yrdA* (rrnD)
KH1141	GGATTTATGAGTGACATGCAACATACTGCCATCCTGCCATGGTCCATATGAATATCCTCC	
KH961	GCGCGAGATTGCCTCCTACCTGGCTTCGGAACTGAAATTGCATGCAGATTGCAGCATTAC	Used with 962 to insert P1-parS at hemG (rrnA)
KH962	AGTTTTCCCACTGTGGTTCTTCAATGCGGTGCACAGCCATGGTCCATATGAATATCCTCC	
KH927	CCATACTGCGCTTCTTTTTATCGCTCATTCAATTGCATGCAGATTGCAGCAGG	Used with 928 to insert pMT-parS at *yieP* (rrnC)

KH928	CTGCTACGCTCACCTGATAAGTGATAACCCGATAAGCCATGGTCCATATGAATATCCTCC	
KH1220	TGGATGGGCGGTGAAATATCCCTGCGTAGTGCAGAAAAATTGCATGCAGATTGCAGCAGG	Used with 1221 to insert pMT-parS at *murI* (rrnB)
KH1221	CTAATCATGCGGTAGAAGAGGTCAGACTACGCAAAGCCATGGTCCATATGAATATCCTCC	
KH1135	AACGGGCAACGCCGTCAATGAAATGGATGTTAAGGTTGCATGCAGATTGCAGCATTACAC	Used with 1136 to insert p1-parS at *gmhB* (rrnH)
KH1136	TTCGCATAAACCTGATTGATTTAGACGTCTGGATGGCCATGGTCCATATGAATATCCTCC	
KH1100	GGCTAGCAGTTGTCCGCCGATCAACGTCACATACTGAAATTGCATGCAGATTGCAGCAGG	Used with 1101 to insert p1-parS at *clpB* (rrnG)
KH1101	TTGCCGTTGAAGGGCGCAAAGGTTTTTACGCATCAGCCATGGTCCATATGAATATCCTCC	
KH1132	CATCTCTTTAATAATGGCGTCATAGTCGCTGCTCTTCACTTGCATGCAGATTGCAGCAGG	Used with 1133 to insert pMT-parS at *purH* (rrnE)
KH1133	CCGCCGCCAAGAACCATAAAGATGTCGCAATCGTGGCCATGGTCCATATGAATATCCTCC	
KH454	GAGCGGATAACAATTCCCCTCTAGA	Used with 455 to generate backbone for pKH2. Template is pCT310
KH455	TCATCGGTATCATTACCCCCATG	
KH456	TTTCTGTTCATGGGGGTAATGATACCGATGACATCGATGCATAATGTGCCTGTC	Used with 455 to generate pAraBAD insert for pKH2. Template is pBAD33-Flp
KH457	TTATTTCTAGAGGGGAATTGTTATCCGCTCCGGGTATGGAGAAACAGTAGAGAG	
KH440	TAGTTCTCAGCCAGAACATACGAA	Used with KH441 to make gRNA insert targeting *yeiP* (rrnC)
KH441	AAACTTCGTATGTTCTGGCTGAGA	
KH442	TAGTCGCGATCTTTTTCCACAAAT	Used with KH443 to make gRNA insert targeting *yrdA* (rrnD)
KH443	AAACATTTGTGGAAAAAGATCGCG	
KH480	TAGTCTATACCGATTGGGAGCAGG	Used with KH481 to make gRNA insert targeting *hemG* (rrnA)
KH481	AAACCCTGCTCCCAATCGGTATAG	
KH482	TAGTCTCGAAAAACTGGCAGTTTT	Used with KH483 to make gRNA insert targeting *murI* (rrnB)
KH483	AAACAAAACTGCCAGTTTTTCGAG	
KH484	TAGTCTGAGCAGAGCGCGGCGGAC	Used with KH485 to make gRNA insert targeting *purH* (rrnE)
KH485	AAACGTCCGCCGCGCTCTGCTCAG	
KH486	TAGTGATAAAAAAGCAGCAAAAAC	Used with KH487 to make gRNA insert targeting *gmhB* (rrn*H*)
KH487	AAACGTTTTTGCTGCTTTTTTATC	

KH488	TAGTTCCGGTCTTCATTAACTTCC	Used with KH489 to make gRNA insert targeting *clpB* (rrnG)
KH489	AAACGGAAGTTAATGAAGACCGGA	
KH451	TAGTGTCACGACGTTGTAAAACGA	Used with KH452 to make gRNA insert targeting *lacZ*
KH452	AAACTCGTTTTACAACGTCGTGAC	
KH337	TAGTCGTTTTACAACGTCGTGACT	Used with KH481 to make gRNA insert targeting *lacZ* (no PAM)
KH338	AAACAGTCACGACGTTGTAAAACG	
KH965	GTTTTTTTGGGCTAGCGAATTCGAGCTCGGCGCACGACACTGAACATACGAATTT	Used with KH966 to generate groEL insert
KH966	TGCAGGTCGACTCTAGAGGATCCCCGGGTAGAGGTGCAGGGCAATTACATCAT	
KH967	TACCCGGGGATCCTCTAGAGTC	Used with KH968 to generate backbone for KH13. Template is pBAD33-Flp
KH968	CCGAGCTCGAATTCGCTAGCC	
KH1012	AAAGCGACATTCTGGCAATTGTTGAAGCGTAATCCGATTACACGTCTTGAGCGATTGTGT	Used with KH1013 to generate PCR product for deletion of *groL*
KH1013	CAGACATTTCTGCCCGGGGGTTTGTTTATTTCTGCGCCATGGTCCATATGAATATCCTCC	
KH1035	CGTTTTTTTGGGCTAGCGAATTCGAGCTCGGTCACCCATAACAGATACGGACTTTC	Used with KH1036 to genrate insert for pKH13
KH1036	CTGTTTTATCAGACCGCTTCTGCGTTCTGATCAAAAGAAAAACCCCCAGACATTTC	
KH1164	ATCAGAACGCAGAAGCGGTCTG	Used with KH1165 to genrate backbone for pKH14
KH1165	ATAGGGTTTGCAGAATCCCTGCTTC	
KH1166	TGGACGAAGCAGGGATTCTGCAAACCCTATTGTCCGATTGCGCCCAAATTTTGG	Used with KH1167 to generate insert for pGroE-GroEL/GroES
KH1167	TGTTTTATCAGACCGCTTCTGCGTTCTGATGGCAATTACATCATGCCGCCC	
KH1214	ATCAGAACGCAGAAGCGGTCTG	Used with KH1215 to generate insert for KH15
KH1215	GAGAAAGTCCGTATCTGTTATGGGT	
KH1216	GCGTCACCCATAACAGATACGGACTTTCTCGCCAGAAGATATCGATTGAGAGGATT	Used with KH1217 to generate insert for KH15
KH1217	TTAAATTCGTATGTTCAGTGTCGTGCGCGGTCCAGGGTTCTCTGCTTAATAGC	
KH1308	ACTTTGCTTCATATGACGAAGCAACC	Used with KH1309 to generate insert for pKH16
KH1309	GCGCCTATATCGCCGACATCAC	
KH1310	GATGTCGGCGATATAGGCGCTTAATCGTCCAGGAAGCTACG	Used with KH1309 to generate backbone for pKH16
KH1311	TTCGTCATATGAAGCAAAGTAAGGACATCGGGTCAATCGCC	

KH1277	CAGCTGGAAAAGAACGCGATGAAAAA	Used with KH1278 to make pKH17
KH1278	GCGTACACGCGCAGCGGAAA	
KH1285	GCGCTGGCCGGACGAAGA	Used with KH1286 to make pKH18
KH1286	GCACGGATGATGTCCTGGCT	
KH1308	TAAAACGCTGAACCTGTCTCACCTG	Used with KH1268 to make pKH19 backbone
KH1309	GCTGCTTCCAGATCGCCATG	
KH1310	GATGTCGGCGATATAGGCGCTTAATCGTCCAGGAA GCTACG	Used with KH1311 to make pKH19 insert
KH1311	TTCGTCATATGAAGCAAAGTAAGGACATCGGGTCAA TCGCC	
KH2215	CTATTAAGCAGAGAACCCTGGATGAGA	Used with KH2216 to make backbone for pKH22-pKH27
KH2216	TCAAATCCTCTCAATCGATATCTTCTGGC	
KH2217	TGCCAGAAGATATCGATTGAGAGGATTTGAATG TCTGACCGCGCCACTAC	Used with KH2219 to make insert for pKH22, and insert for pKH27
KH2218	GATTCTCATCCAGGGTTCTCTGCTTAATAGTCAT AACCCATACTCCAGACGGAA	
KH2219	TGCCAGAAGATATCGATTGAGAGGATTTGAATG AGTCAGAATACGCTGAAAGTTCATG	Used with KH2221 to make insert for pKH23
KH2220	GTTCTGATTCTCATCCAGGGTTCTCTGCTTAATA GTTACTCGCGGAACAGCGCTT	
KH2221	TGCCAGAAGATATCGATTGAGAGGATTTGAATG AGCGAGCAGTTAACGGACC	Used with KH2223 to make insert for pKH24
KH2222	GATTCTCATCCAGGGTTCTCTGCTTAATAGTCAA CGCCTGATAAGCGGTTGAAC	
KH2223	TGCCAGAAGATATCGATTGAGAGGATTTGAATG AAGCAAGGTTTGCAACTCAGG	Used with KH2225 to make insert for pKH25
KH2224	GATTCTCATCCAGGGTTCTCTGCTTAATAGTCAA ACGAGTTGTTTACGCTGGTTTG	
KH2225	TGCCAGAAGATATCGATTGAGAGGATTTGAGTG AATTCACTCTATACCGCTGAAGG	Used with KH2227 to make insert for pKH26
KH2226	GATTCTCATCCAGGGTTCTCTGCTTAATAGTTAT AACTTACCCAGTTTAGTGCGTAACC	
KH1262	TTTTTTTGTCCGCCAGGATCCAGGCGTGATCCG CAATACTTAACACTTCCTCCTAATTTTTGTTGACA CTCTATC	Used with KH1263 to generate PCR product to insert *attP* into *mlaF*
KH1263	TTTCCCTTTGATGGCACATCGTGAGAAACCACC ACACAAGTCACGCCCAGCGCGCTGTTCAGGA TGGTCGGGTTTAACGTTCATT	
KH1717	TTTTTGCGGCCGCAAGATCCG	Used with KH1672 to make backbone for KH20
KH1672	TGATGTTATTCCGCGAAATATAATGACCCT	
KH1716	GTTGAACTGCGGATCTTGCGGCCGCAAAAATGATGT TATTCCGCGAAATATAATGACCCT	Used with KH1675 to make insert for KH20

KH1675	AGGGTCATTATATTTCGCGGAATAACATCAGATGGTCGGGTTTAACGTTCATT	
KH1447	CCATCGGTGATGTCGGCGATATAGGCGCATTTCACCGTCATCACCGAAACGC	Use with 1448 to make insert for KH19
KH1448	TTCAAATCCTCTCAATCGATATCTTCTGGCCGAGCTCGAATTCCATGGTCTGTTTC	
KH1449	GCCAGAAGATATCGATTGAGAGGATTTGA	Use with 1448 to make backbone for KH19

Table 2. Primers used in this study.